AFOSR-TR. 91 0495

TRANSPIRATION COOLED
ULTRAVIOLET
SOL-GEL SILICA OPTICS

DTIC
ELECTE
MAY 08 1991
S
C
D

GELTECH

SBIR PHASE I FINAL TECHNICAL REPORT
PREPARED FOR
AIR FORCE OFFICE OF SCIENTIFIC RESEARCH
BOLLING AFB, DC 20332

The views and conclusions contained in this document are those of the authors and should not be interpreted as necessarily representing the official policies or endorsements, either expressed or implied, of the Air Force Office of Scientific Research or the U.S. Government.

91 5 06 173

REPORT DOCUMENTATION PAGE

1a. REPORT SECURITY CLASSIFICATION UNCLASSIFIED		1b. RESTRICTIVE MARKINGS			
2a. SECURITY CLASSIFICATION AUTHORITY		3. DISTRIBUTION / AVAILABILITY OF REPORT			
2b. DECLASSIFICATION / DOWNGRADING SCHEDULE		Approved for public release; distribution unlimited.			
4. PERFORMING ORGANIZATION REPORT NUMBER(S) FINAL TECHNICAL REPORT		5. MONITORING ORGANIZATION REPORT NUMBER(S)			
6a. NAME OF PERFORMING ORGANIZATION GELTECH, INC.	6b. OFFICE SYMBOL (If applicable)	7a. NAME OF MONITORING ORGANIZATION Air Force Office of Scientific Research			
6c. ADDRESS (City, State, and ZIP Code) Two Innovation Drive Alachua, FL 32615		7b. ADDRESS (City, State, and ZIP Code) Building 410 Bolling AFB, DC 20332-6448			
8a. NAME OF FUNDING / SPONSORING ORGANIZATION AFOSR	8b. OFFICE SYMBOL (If applicable) NC	9. PROCUREMENT INSTRUMENT IDENTIFICATION NUMBER F49620-90-C-0055			

8c. ADDRESS (City, State, and ZIP Code) Building 410 Bolling AFB, DC 20332-6448	10. SOURCE OF FUNDING NUMBERS			
	PROGRAM ELEMENT NO. 65503F	PROJECT NO. 3005	TASK NO. A1	WORK UNIT ACCESSION NO.

11. TITLE (Include Security Classification)

Transpiration Cooled Ultraviolet Sol-Gel Silica Optics

12. PERSONAL AUTHOR(S)
Dr. Vinay K. Seth and Dr. Jean-Luc R. Nogues

13a. TYPE OF REPORT Final Technical	13b. TIME COVERED FROM 90-08-15 TO 91-03-15	14. DATE OF REPORT (Year, Month, Day) 91-04-01	15. PAGE COUNT 68

16. SUPPLEMENTARY NOTATION

17.	COSATI CODES		18. SUBJECT TERMS (Continue on reverse if necessary and identify by block number)
FIELD	GROUP	SUB-GROUP	Transpiration cooling, Sol-Gel, Porous Silica, Rocket
			Window, Ultraviolet Transmission

19. ABSTRACT (Continue on reverse if necessary and identify by block number)

All rocket guidance systems essentially require broad-band optical transmission windows. These windows must also be temperature insensitive to transmission, thermal shock resistant, thermally stable, reasonably strong, and impact resistant. At hypersonic velocity convective cooling is preferred to radiative cooling. Transpiration cooling is a novel and effective mode of convective cooling. Porous silica windows offer excellent rocket windows for transpiration cooling at a relatively inexpensive price. Sol-gel technology is an enabling technology which facilitates the fabrication of these rocket windows. This research used sol-gel technology to demonstrate the concept of transpiration-cooled porous silica windows. These windows were fabricated with various pore sizes and characterized with respect to gas diffusion, transpiration, high temperature transmission, thermal stability and shock resistance, hardness, impact resistance, and strength. The manufacturability aspect was also addressed. The diffusion of various gases through porous silica windows was studied and their permeabilities measured. In the experimental range, Knudsen diffusion seemed to be the predominant mass transport mechanism. At a low transpiration velocity of 0.52 cm/s of helium, a 44°C temperature drop was observed showing the promise of this material for rocket window application. High temperature spectroscopy showed improved performance.. The porous silica windows had thermal stability and thermal shock resistance and reasonable mechanical properties. This proof-of-concept research demonstrates the feasibility of porous silica windows for transpiration-cooled optics of rocket guidance systems.

20. DISTRIBUTION / AVAILABILITY OF ABSTRACT ☒ UNCLASSIFIED/UNLIMITED ☒ SAME AS RPT ☐ DTIC USERS	21. ABSTRACT SECURITY CLASSIFICATION UNCLASSIFIED	
22a. NAME OF RESPONSIBLE INDIVIDUAL Mr. Charles Lee	22b. TELEPHONE (Include Area Code) (513)255-9155	22c. OFFICE SYMBOL NC

DD FORM 1473, 84 MAR — 83 APR edition may be used until exhausted. — SECURITY CLASSIFICATION OF THIS PAGE
All other editions are obsolete.

UNCLASSIFIED

ACKNOWLEDGEMENTS

EXECUTIVE SUMMARY

All rocket guidance systems essentially require broad-band optical transmission windows. These windows must also be temperature insensitive to transmission, thermal shock resistant, thermally stable, reasonably strong, and impact resistant. At hypersonic velocity convective cooling is preferred to radiative cooling. Transpiration cooling is a novel and effective mode of convective cooling. Porous silica windows offer excellent rocket windows for transpiration cooling at a relatively inexpensive price. Sol-gel technology is an enabling technology which facilitates the fabrication of these rocket windows. This research used sol-gel technology to demonstrate the concept of transpiration-cooled porous silica windows. These windows were fabricated with various pore sizes and characterized with respect to gas diffusion, transpiration, high temperature transmission, thermal stability and shock resistance, hardness, impact resistance, and strength. The manufacturability aspect was also addressed. The diffusion of various gases through porous silica windows was studied and their permeabilities measured. In the experimental range, Knudsen diffusion seemed to be the predominant mass transport mechanism. The effects of transpiration cooling were studied in greater detail using helium gas. At a low transpiration velocity of 0.52 cm/s of helium, a 44°C temperature drop was observed showing the promise of this material for rocket window application. High temperature spectroscopy showed improved performance, especially for 25 Å pore diameter windows. The thermal stability and thermal shock resistance of the windows was excellent irrespective of the pore size. The porous silica windows had reasonable mechanical properties. This proof-of-concept research demonstrates the feasibility of porous silica windows for transpiration-cooled optics that can be used in rocket guidance systems.

OBJECTIVES OF THE RESEARCH EFFORT

The specific objectives of the Phase I effort were:

1. To determine the diffusion characteristics of various gases through porous silica. The pore size and the pore distribution were changed so as to see its effects on the diffusion characteristics of various gases. This impacts directly on the performance characteristics of the windows.

2. To study the variation of the transpiration rate of various gases through porous silica. Also included in this study was the effect of the actual pore size. The emphasis was on large pore diameter porous silica windows, as the ultimate goal here was to fabricate rocket windows with a high transpiration rate.

3. To study the porous silica material of various pore diameters for their UV transmission characteristics. The importance of this study lies in the fact that this rocket window has the potential to expand the useful spectrum. Also, during in-flight conditions the temperature of the window increases due to air friction which can affect the critical transmission characteristics.

4. To determine the suitability of the porous silica windows for rocket windows with respect to their thermal shock and thermal stability. The importance of these thermal properties is underscored by the fact that the skin temperature of the projectile at hypersonic velocity reaches hundreds of degrees Celsius in a relatively short period of time.

5. To study the mechanical properties of the rocket windows of various pore diameters. The impact strength and the surface hardness of the rocket windows are important parameters as these hypersonic projectiles will encounter hydrometeors

and airborne particles during deployment. The ultimate goal of this study was to determine the suitability of the porous silica windows in terms of their mechanical properties.

LIST OF PUBLICATIONS RESULTING
FROM THIS RESEARCH EFFORT

1.　A. Fozmoe and L.L. Hench, "Gas Permeability in Porous Gel-Silica," *5th International Conference on Ultrastructure Processing*, Feb. 17-21, 1991, Orlando, FL.

A copy of this publication is provided in Appendix A.

LIST OF PROFESSIONAL PERSONNEL ASSOCIATED WITH THE RESEARCH EFFORT

Technical Staff

Jean-Luc R. Noguès - Principal Investigator and Vice President R&D

Vinay K. Seth - Research Scientist

William V. Moreshead - Research Scientist

Bing-Fu Zhu - Research Scientist

Fred Chapman - Group Support Engineer

James Callahan - Technician

Letha Rice - Technical Writer

Corporate Staff

Anthony J. LaPaglia - President & CEO

Joseph L. Lombardi - Secretary and Controller

LIST OF TABLES

LIST OF FIGURES

TABLE OF CONTENTS

RESEARCH REPORT

1. INTRODUCTION

1.1 Requirements for Rocket Windows

All ballistic missile interceptors and their targets like intercontinental ballistic missiles (ICBMs) and ballistic re-entry vehicles (BRVs) utilize rocket guidance systems that require transmission windows for broad-band optical transmission. Apart from good transmission characteristics, the rocket window materials must be temperature-insensitive to transmission, have high thermal shock resistance, high thermal stability, reasonable structural strength and good impact strength [1].

The transmission characteristics of the window materials are critical as they must permit the registration of visible and infrared (IR) optical signatures. The current trends are to expand the spectral range into the ultraviolet (UV) range, and to enhance the transmission quality of the windows. During projectile flight the temperature of the window will vary due to atmospheric friction from interaction with hydrometeors (ice, small snow, large snow, rain, etc.) and with high-altitude cirrus encountered. Hence, the optical transmission characteristics of the window material should have immunity to temperature. The window material should have high thermal shock resistance due to small time intervals in which hypersonic velocity (greater than Mach 5) can be attained and atmospheric variations encountered. High thermal stability is required for the windows as they are integrated as a component of a larger system that needs to be relatively temperature-insensitive. Reasonably good mechanical strength is a necessity for these transmission windows due to in-flight conditions which may include airborne vibrations. The impact strength of the window material must be satisfactorily high as the projectile velocity will be hypersonic and the window will encounter hydrometeors and various kinds of airborne particles which have varying size distributions. As per the requirements above, the ideal candidate materials for rocket windows are sapphire and diamond. These materials, however, are difficult to manufacture (especially in the

required shapes and sizes) and are extremely expensive and cost prohibitive.

As the rocket window is a critical component of the guidance system, there exists a need for a material which can be processed into the required shapes and sizes, and have the properties mentioned above – all at a relatively low price.

1.2 Heat Transfer in Rocket Windows

In its trajectory, a projectile has a shock wave preceding it that is in the form of a cone (Mach cone). The skin temperatures of the projectile at a hypersonic velocity are a few hundred degrees Celsius, depending on the site on the structure. An intense thermal boundary exists adjacent to the exterior (exposed) surface of the window [1]. Due to the temperature dependence of the bandpass of the window, any change in the temperature of the window occurring due to radiative and convective heat transfer from the boundary layer will dramatically affect optical transmission. In general, such conditions deteriorate the optical transmission performance of the window.

Figure 1 shows a schematic of heat transfer rates due to convective and radiative processes at various Mach numbers [1]. Note that the vertical scale is logarithmic. Hence, at Mach numbers less than 30, convective processes dominate the radiative ones. While radiative heat transfer can be decreased with a reflective surface, the net heat transfer will be a small percentage of the total heat transfer. Clearly, convective heat transfer mode is preferred to radiative heat transfer mode. An alternative and more effective way of cooling rocket windows is to use transpiration cooling.

1.3 Transpiration Cooling of Porous Rocket Windows

Transpiration is a very effective way of cooling porous structures. In this process, a fluid is forced through a porous plug which results in film cooling at the exterior interface. For cooling of porous rocket windows a gaseous fluid is expected to provide significant cooling effect. The cooling occurs mainly due to continual removal of heat
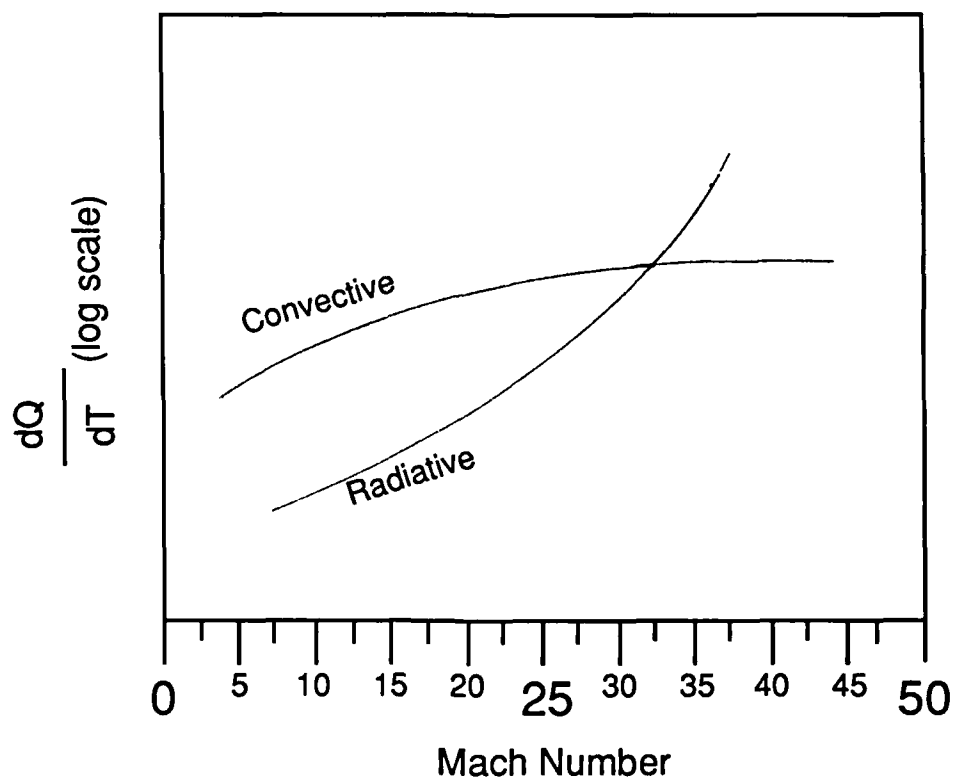
Figure 1. Schematic of Heat Transfer Rate due to Convective and Radiative Processes at Various Mach Numbers.

by rapid outflow of gas, and also due to the expansion of the escaping gas (Joule-Thomson effect).

The net effect of gas transpiration is that it displaces the thermal boundary layer away from the exterior (exposed) surface of the window. This essentially reduces the boundary layer temperature gradient with respect to the distance from the surface. The conduction rate is lowered dramatically as a result of this boundary layer displacement. Transpiration velocities as low as 1.0 cm/s lead to a significant cooling effect.

The Joule-Thomson effect is a phenomenon in which a lowering of temperature occurs when a gas is made to expand adiabatically from a region of high pressure into a region of low pressure. Joule-Thomson coefficient, μ_J, is defined for a gas as the temperature change produced per pressure drop under constant enthalpy conditions when it is passed through a porous plug [2]:

$$\mu_J = [\ \partial T / \partial P\ ]_h$$

This coefficient is itself a property of a substance. Also, μ_J is a function of temperature and pressure and is not a constant. It should be remembered that μ_J can be positive, negative, or zero for real gases, depending on their thermodynamic state. However, a porous media is required which has all the properties discussed earlier (Section 1.1). Porous silica windows match all of the above requirements. Sol-gel technology is an enabling technology in that it facilitates the fabrication of these rocket windows at a relatively low cost.

1.4 Sol-Gel Fabrication of Rocket Windows

Recent developments in sol-gel glass technology have permitted the fabrication of silica glasses at much lower temperatures than traditional melt glass techniques [3]. A schematic representation of the process is given in Figure 2. In this process a silicon-containing precursor, such as tetramethylorthosilicate (TMOS) or tetraethylorthosilicate

```
┌──────────────────┐  ┌──────────────┐  ┌──────────────┐
│ Silicon Precursor│  │  D.I. Water  │  │  Additives   │
└──────────────────┘  └──────────────┘  └──────────────┘
              │              │              │
              └──────────┐   │   ┌──────────┘
                         ▼   ▼   ▼
                      ┌──────────────┐
                      │   Batching   │
                      └──────────────┘
                             │
                             ▼
                      ┌──────────────┐
                      │    Mixing    │
                      └──────────────┘
                             │
                             ▼
                      ┌──────────────┐
                      │     SOL      │
                      └──────────────┘
                             │
                             ▼
                      ┌──────────────┐
                      │    Aging     │
                      └──────────────┘
                             │
                             ▼
                      ┌──────────────┐
                      │   Drying     │
                      └──────────────┘
                             │
                             ▼
                      ┌──────────────┐        ╭────────────────────╮
                      │ Stabilization│──────▶ │ Porous Silica Window│
                      └──────────────┘        ╰────────────────────╯
                             │
                             ▼
                      ┌──────────────┐
                      │Dehydroxylation│
                      └──────────────┘
                             │
                             ▼
                      ┌──────────────┐        ╭────────────────────╮
                      │ Densification│──────▶ │ Dense Silica Window │
                      └──────────────┘        ╰────────────────────╯
```
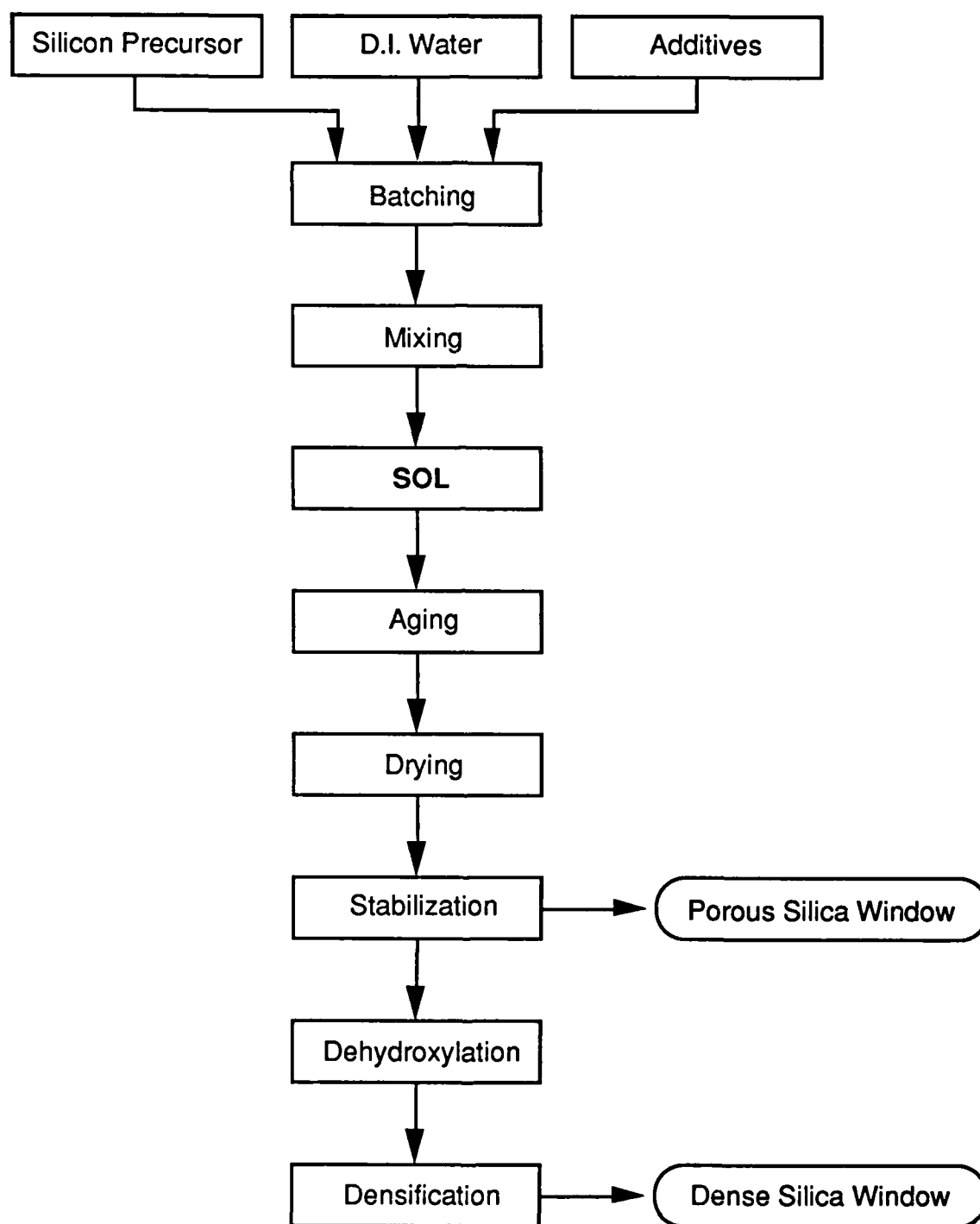
Figure 2. Flowsheet of Sol-Gel Processing of Silica Glass Monoliths.

(TEOS), is hydrolyzed to form a sol. After complete homogenization, this sol is cast into molds where it sets into a very porous, wet, gel having the shape of the mold. The gel is then dried to give a transparent silica monolith. The resulting dry gel can be further heat-treated or stabilized to strengthen it and at the same time reduce its porosity. An ultraporous silica monolith, designated Type VI silica, that can be used as a transpiration rocket window is obtained.

Although stabilization removes most of the water, heating to temperatures necessary to fully densify the silica gel normally results in bloating of the sample due to residual water being trapped in the porous structure. If a dehydration step is carried out before the final densification the bloating problem is avoided and fully dense glass can also be obtained [4], which is designated as Type V silica.

The use of sol-gel processing to prepare rocket windows holds potential advantages for the following reasons:

1. This sol-gel derived silica has an ultraporous structure for gas transpiration. The pore size and total pore volume (pore morphology, in general) is controllable by modification of the processing steps.

2. The broad-band optical transmission is observed for this material. It must be noted that the UV cutoff for densified sol-gel silica is the lowest obtainable.

3. The thermal stability and thermal shock resistance of this material is good. These properties are attributed to silica.

4. The mechanical strength of this material is reasonable. It is dependent on the required pore size and the bulk density of the porous silica.

5. A variety of shapes and sizes of windows can be fabricated by this technique without any major modification of the fabrication process.

6. The cost of these transmission windows is expected to be only a small percent of the cost of the materials currently being used for rocket window applications.

2. EXPERIMENTS

2.1 Fabrication and Characterization of Porous Silica Windows

The raw materials used for fabrication of porous silica windows were tetramethylorthosilicate (TMOS) or tetraethylorthosilicate (TEOS), D.I. water, and proprietary additives. The sols were batched according to the requirements and mixed in a reactor. This sol was cast in polypropylene containers and the lids sealed. These containers were left undisturbed for various lengths of time at temperatures of between 25°C and 80°C during which time the sol gelled into a viscoelastic solid. After gelation these wet gel monoliths were dried to yield crack-free transparent monoliths of the desired shape.

To remove the organic fractions from the gel, a heat treatment step called stabilization was carried out at various temperatures, all below 1200°C. Monoliths of various specific pore sizes were produced. Pore analysis was carried out using a Quantachrome Autosorb-6, which gave average pore diameter, pore size distribution, specific surface area, and specific (total) pore volume.

2.2 Measurement of Diffusion Characteristics

Figure 3 shows the schematic of the apparatus used to measure the transpiration flow of gases through porous media. The setup essentially consisted of a closed chamber with a gas inlet and with the porous silica window as the outlet. A Campbell Scientific CR 10 datalogger was used for monitoring the pressure transducer output. All samples were dry polished on an 18.0 μm grit size sandpaper. The final sample thickness was kept at 2.0 mm during the experiment. This thickness was varied for measurements that involved the thickness of the porous silica window as the parameter.

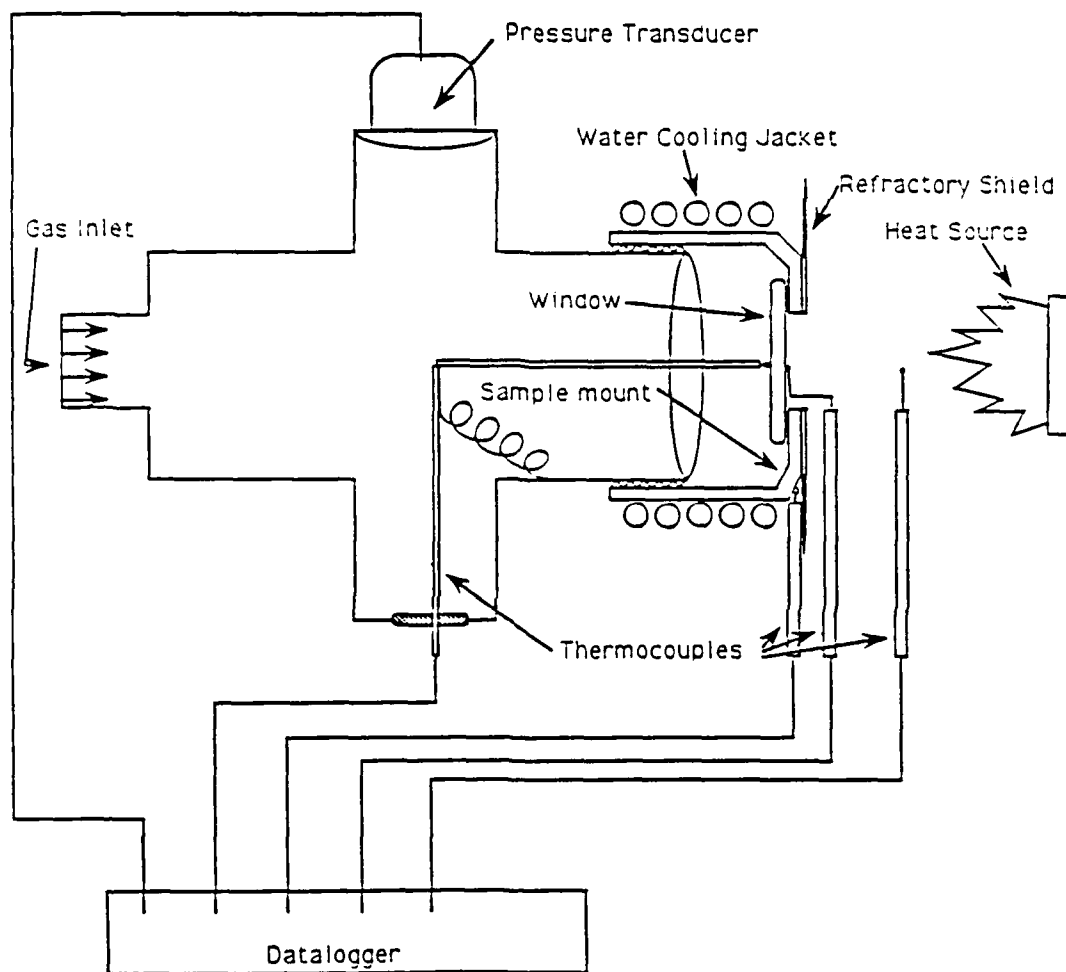All samples were outgassed by heating in a vacuum oven before the measurements were

Figure 3. Schematic of the Apparatus for Transpiration Cooling Measurement.

made. A soap bubble flow meter was used for calibration of flow rate. The gas used was Helium with a 99.99% purity. Each sample of specified thickness and pore structure had a corresponding calibration curve.

2.3 Measurement of Transpiration Characteristics

The chamber used for studying the diffusion characteristics was also used for measurement of transpiration characteristics. Five K-type thermocouples were added on to the CR 10 datalogger as shown in Figure 3. The location of the thermocouples was selected systematically. Thermocouples #1 and #2 measured interior and exterior (exposed to atmosphere) surface temperatures of the window, respectively. The ambient and the heat source temperatures were measured by thermocouples #3 and #4 respectively. As a precautionary measure, a separate thermocouple measured the temperature of the sample mount. An Omegalux CIR series high watt density heating cartridge was used as a heat source.

The test was carried out in the following manner. A steady state flow velocity was obtained with a direct heating of the surface, which left the surface at a constant high temperature. This dynamic equilibrium state was disrupted by bringing the flow rate to zero. A new equilibrium state was achieved with new temperature readings. The flow rate was increased to its original value and the experiment repeated. All changes in temperatures and pressure were recorded.

The sample preparation was done as described in section 2.2. The flow rate calibration made earlier was used for studying the transpiration characteristics.

2.4 High-Temperature Transmission Spectroscopy

Two kinds of experimental setups were used to study the high temperature transmission spectra of porous silica windows with varying pore diameters – one in which the window was heated by an oxygen-acetylene flame, and the other wherein the window

was heated in a conventional oven.

Figure 4 shows the setup for high-temperature transmission spectroscopy of porous silica windows using an oxygen-acetylene flame. This apparatus included a light source, a sample holder with attached thermocouple, an oxygen-acetylene torch, and a UV detector. The samples were fixed in the sample holder and heated using the oxygen-acetylene torch.

The setup for high-temperature spectrophotometry of the transpiration window built for a conventional furnace is shown in Figure 5. Both the sample holder and the baseplate were made out of high heat capacity firebrick to slow down the heat loss due to ambient convection and radiation. The whole assembly, including the sample, was heated in a conventional oven and then placed in the analysis chamber of the spectrophotometer. The temperature of the sample at the start of the experiment was selected so that after the run was complete the average temperature was 400° C.

2.5 Testing of Thermal Properties

2.5.1 Thermal Stability

The thermal stability of the porous silica window depends on the matrix material, which is silica, and the nature of its porosity. Sol-gel derived porous silica windows have open, interconnected porosity. The material is expected to be thermally stable. Dilatometry was conducted previously on such porous samples.

2.5.2 Thermal Shock Resistance

Thermal shock testing was carried out from the following temperatures: 25°C, 100°C, 200°C, 300°C, 400°C, and 500°C. The procedure essentially involved heating the sample in a furnace (see Figure 6) for 30 minutes followed by quenching (similar to ASTM C149-86). Various pore diameter porous silica samples were quenched in air
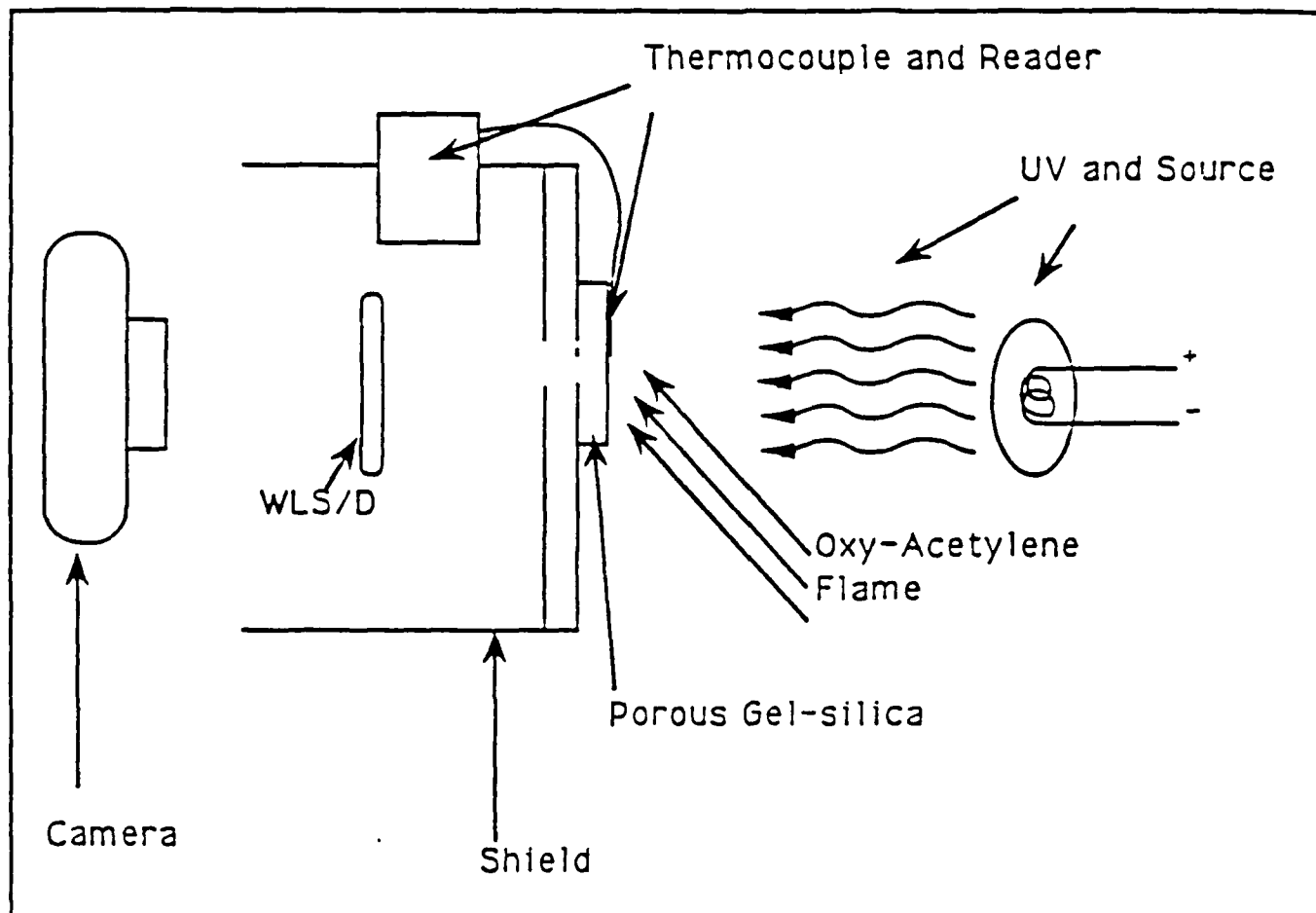
Figure 4. High-Temperature Spectroscopy of Porous Silica Windows Using Oxygen-Acetylene Flame.
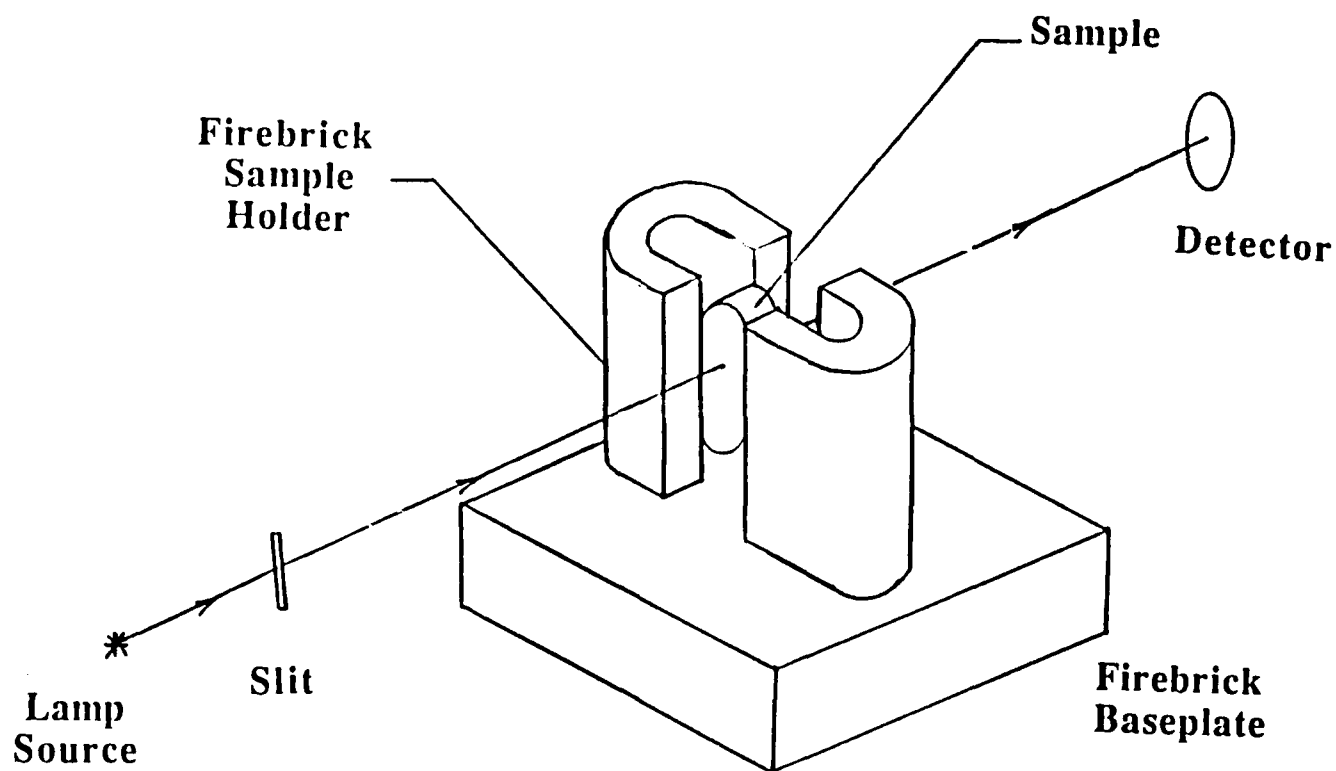
Figure 5. High-Temperature Spectroscopy of Porous Silica Windows Using Conventional Furnace.

(25°C), mist (15°C), water (15°C), and liquid nitrogen (-77°C).

2.6 Testing of Mechanical Properties

2.6.1 Vicker's Hardness

Vicker's hardness number was obtained from a diamond pyramid hardness test. The load divided by surface area of the indentation provides the number in units of kg/mm^2. A Leco DM-400F hardness tester was used with an initial load of 0.1 kg with indentation dwell time of 20 s. The loads and the dwell times were changed so as to obtain good measurable indentation marks on porous silica windows of various pore diameters.

2.6.2 Impact Testing

The impact testing was conducted in accordance with ASTM C368-77 (reapproved 1982). The impact tester, as shown in Figure 7, was pendulum type in which a steel tup of specified size and Rockwell hardness C 55 hits the sample after it (the tup) is released from a fixed height. Samples of porous silica windows of various pore diameters were tested.

Platinum wire

Furnace

Sample

Liquid Bath
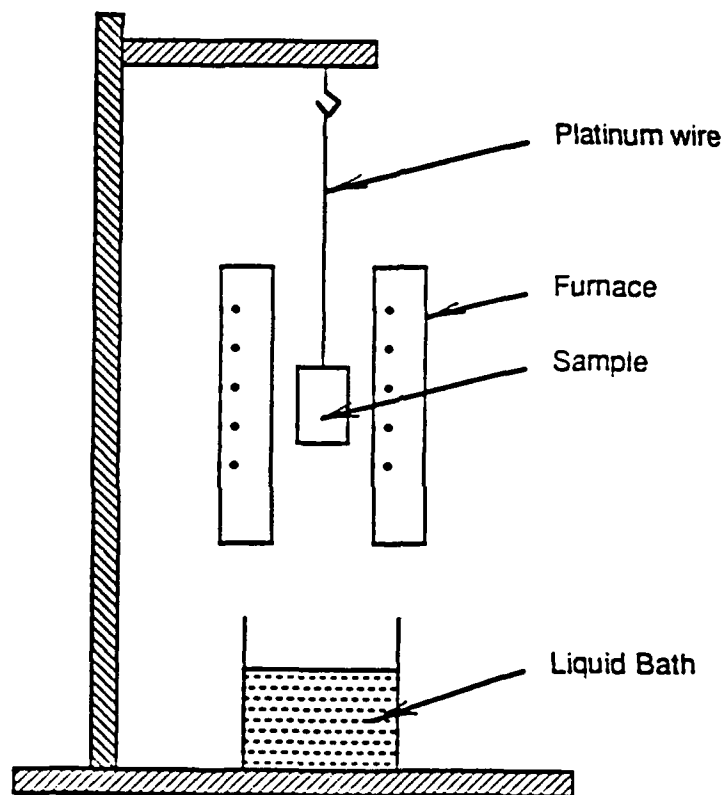
Figure 6. Setup for Thermal Shock Testing.

Side Elevation of Assembly

A—Handwheels.
B—Pendulum support bar.
C—Backstop.
D—Tup.

E—Angle clamp.
F—Positioning arm
G—Triangular castings for specimen supports.
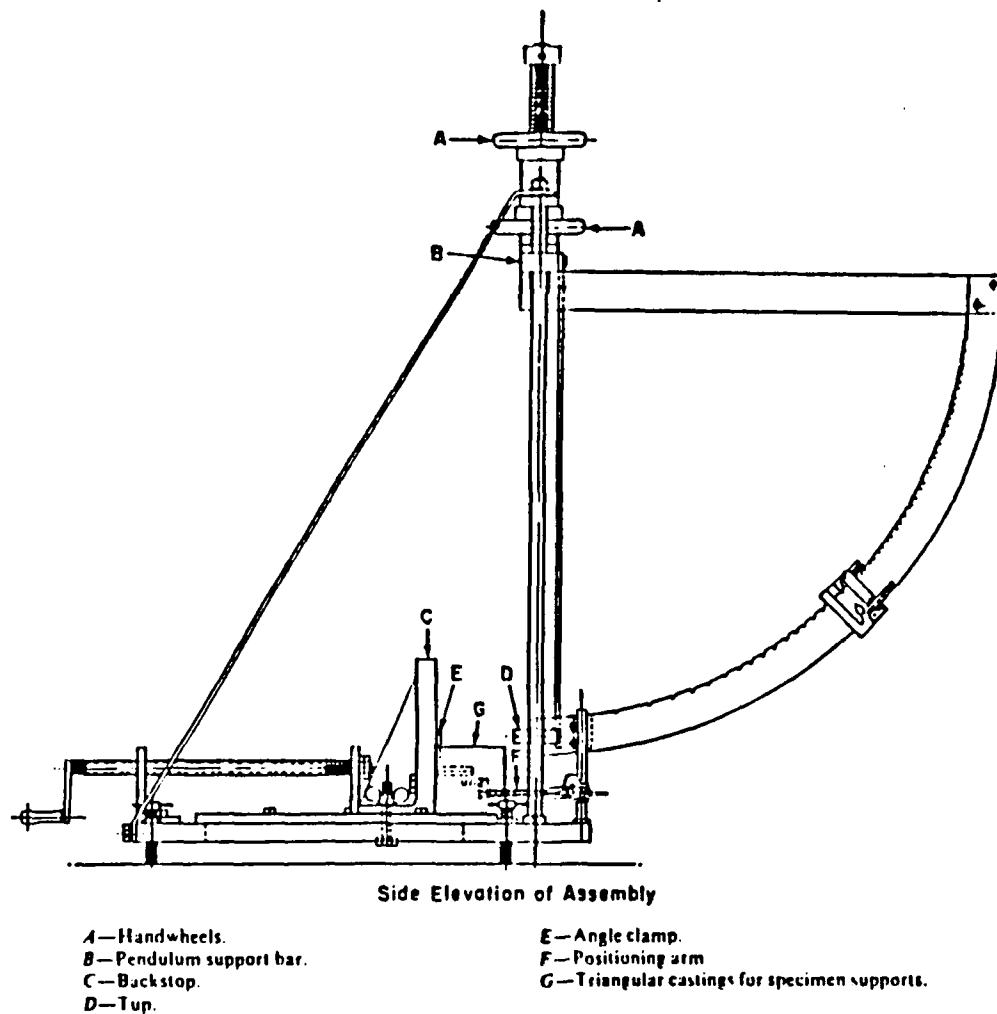
Figure 7. Impact Testing Apparatus.

3. RESULTS AND DISCUSSION

3.1 Characteristics of Various Pore Diameter Porous Silica Windows

The drying and heat treatment schedules essentially control the ultrastructure of porous silica windows. The temperature of heat treatment is an important parameter. Figure 8 shows the evolution of the ultrastructure-dependent characteristics as a function of temperature [5]. As the temperature increases, the specific surface area and the total pore volume decrease. Note the sharp declines around 900°C for a 25 Å pore diameter porous silica.

Figure 9 shows the comparison of characteristics of 25 and 160 Å pore diameter porous silica as a function of temperature. Notice that the pore radius is independent of the processing temperature. Also, both the surface area per unit volume and volume fraction porosity are relatively insensitive to temperature up to about 900°C. Beyond this temperature, there is a steep decline in the values of surface area per unit volume and volume fraction porosity for 160 Å pore diameter, just as for 25 Å pore diameter porous silica [6]. The pore size distribution is also narrow and within one decade [6].

The large pore radius porous silica has a low surface area per unit volume as shown in Figure 9. The theory of viscous sintering is based on an assumption that energy dissipation in viscous flow is equal to the energy gained by the decrease in surface area during densification [7]. Hence, the driving force for viscous sintering of 160 Å pore diameter silica is lower than that for 25 Å pore diameter silica. Thus, the porous silica with larger pore diameter must be taken to a higher temperature to obtain similar volume fraction porosity as shown in Figure 9(b).

The yield of the porous silica windows during manufacture must be addressed at this stage. It was noted that the 112 Å pore diameter porous windows had a significantly lower yield than the 25 Å pore diameter windows. This is most likely due to the lower
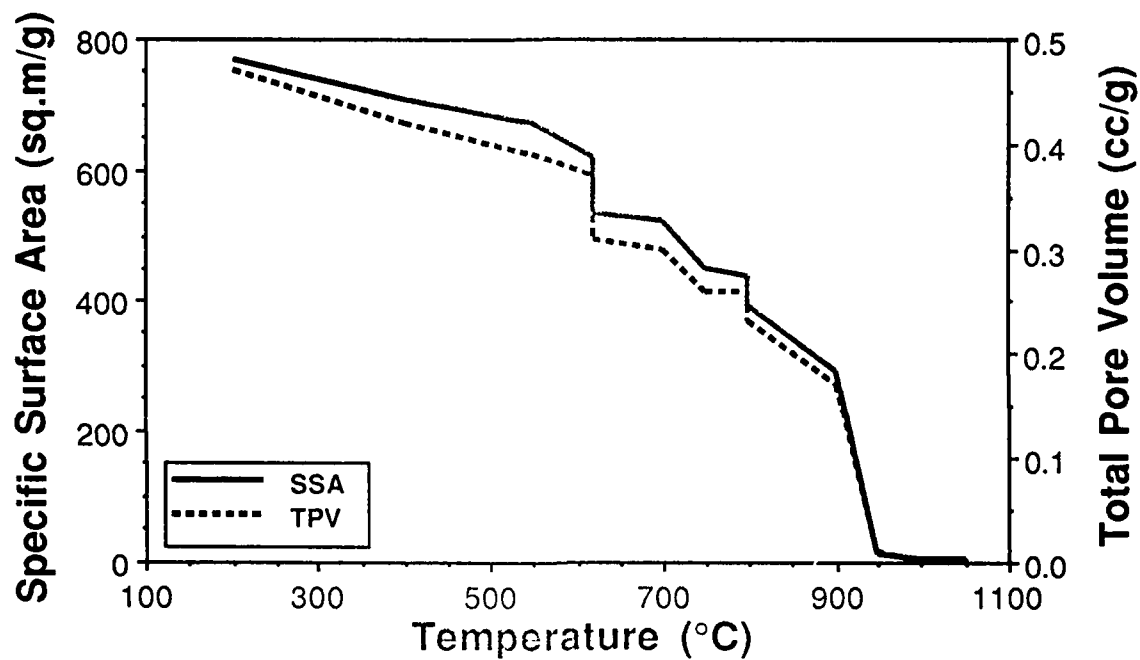
Figure 8. Change in Specific Surface Area and Total Pore Volume of Sol-Gel Silica with Heat Treatment.
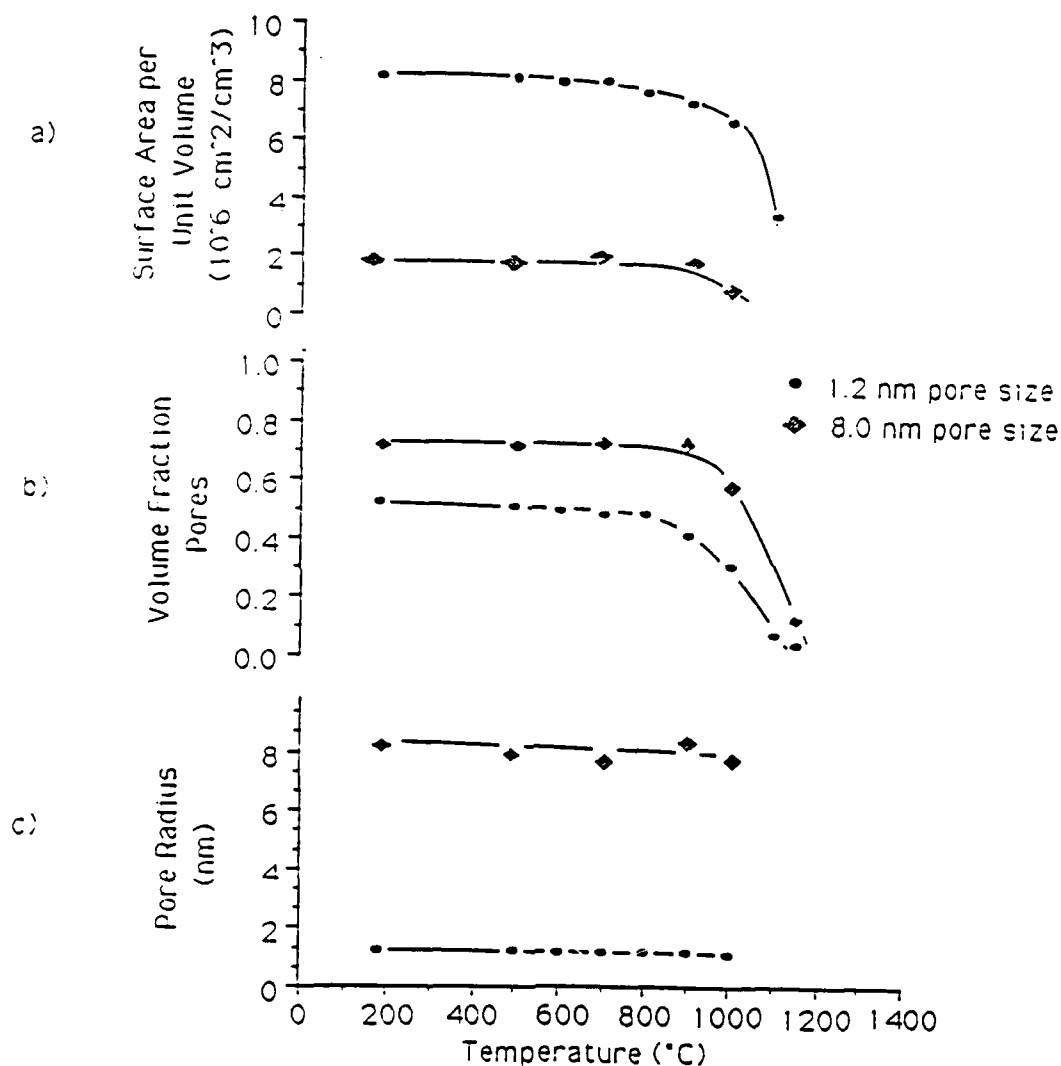
Figure 9. Variation of Pore Morphology with Temperature of Heat Treatment for Sol-Gel Silica.

mechanical strength of the larger pore diameter windows.

3.2 Gas Diffusion through Porous Silica Windows

The diffusion or permeation of a fluid, gas, or liquid through a porous solid involves two basic resistances to the net flow velocity of a given species [8]. These are molecule-molecule and molecule-wall interactions. The part each of these interactions plays in determining the flux of a species is dependent on the parameters of both the fluid and the porous network.

The parameters of the porous network (pore morphology) ? which can play a large part in determining the flux include the effective porosity (interconnected porosity), pore size of the channels, pore size distribution, specific surface area (ratio of the internal surface area to volume), tortuosity of the channel, and surface roughness of the channel, to name a few [8]. Important parameters of the fluid (in this case gas) include properties such as viscosity, temperature, and the molecular weight of the species.

The diffusion of gases through porous silica windows with different pore diameters directly affects transpiration cooling. The passage of the fluids through a porous media will not result in straight streamlines of flow. Indeed if the porosity has high tortuosity, like the interconnected pores of sol-gel derived porous silica windows, then a percentage of total gas flow will not go straight through the sample as shown schematically in Figure 10. This tortuosity can be translated into the total surface area of the porous media exposed to the gas and to the thickness of the media which the gas encounters during its passage from a high pressure to a low pressure region.

Figure 11 depicts the transpiration flow rate of helium through 24 and 160 Å pore diameter silica windows as a function of pressure [9]. Two different processing temperatures were used, 180°C and 500°C. The samples processed at the higher temperature (500°C) had a lower surface area per unit volume (constant geometry) and a lower volume fraction porosity. It must be pointed out that temperature changes pore
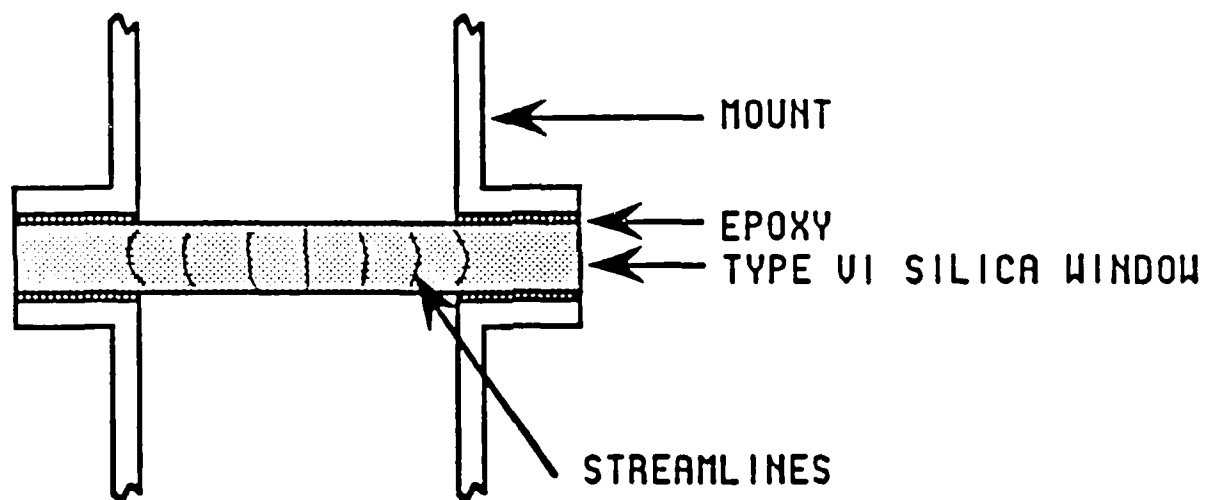
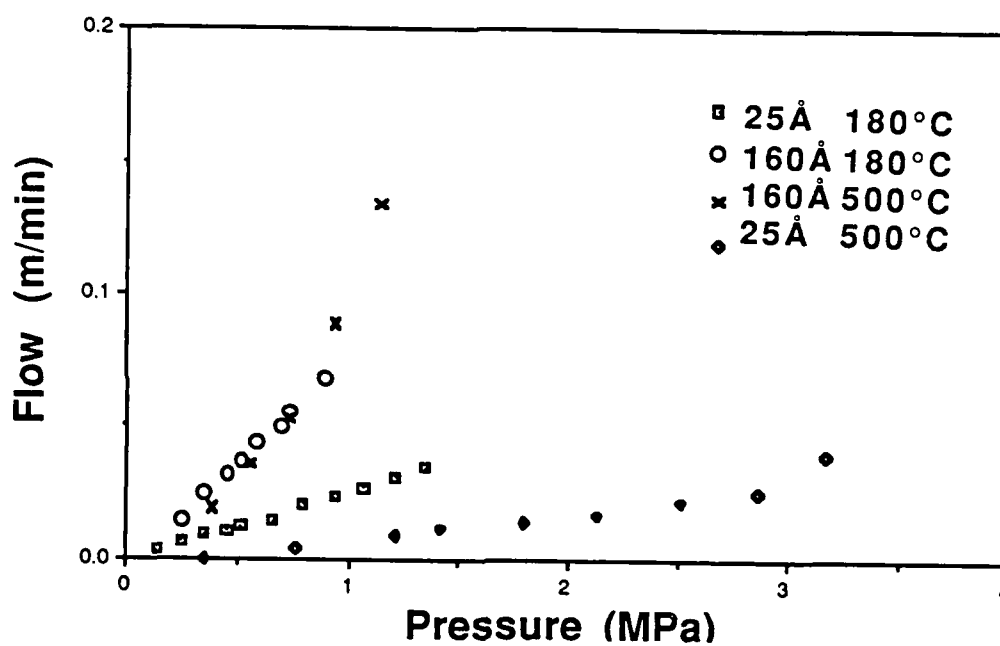**Figure 10. Schematic of Flow Streamlines in a Porous Silica Window.**

Figure 11. Helium Transpiration Rate Through 24 Å and 160 Å Pore Diameter Silica Gels as a Function of Pressure.

morphology (in terms of interconnectivity) but not pore size. As is evident from Figure 11, at a constant pressure the transpiration flow is higher for larger pore diameter porous silica windows, as expected, due to a higher gas diffusion rate. At the relatively low pressures used for this study the transpiration flow is linear with pressure. It should be noted that the nonlinearity does occur at a lower pressure for higher pore diameter silica. Also, the temperature of heat treatment hardly changes the gas diffusion through larger pore diameter porous silica windows.

The diffusion of a gas depends not only on the pore size and pore connectivity of the medium, but also on the nature of the gas. The gas type and its pressure influence gas diffusion dramatically. To study gas flow through a microporous medium a comparison of the mean free paths (λ) of various gases must be made with the average pore diameter (d) of the media. The kinetic theory of gases relates λ (of a perfect gas) to the mean speed of a molecule (c) and the collision frequency (z):

$$\lambda = c/z = (1/2^{1/2} \sigma) kT/P$$

where σ is the collision cross section, k is the Boltzman constant, T is the temperature, and P is the pressure [10]. Figure 12 shows the mean free paths of various gases as a function of pressure [9].

Due to the complexity of the interconnected pore space in porous silica windows, it is difficult to assign a value to the pore size because of the random converging and diverging of the normal cross section of the pores [8]. The measure of average pore size selected for a porous medium is the hydraulic radius (r_h), which is defined as twice the pore volume divided by the surface area. The method used herein to obtain the hydraulic radius and pore size distribution was isothermal nitrogen gas adsorption-desorption technique, interpreted using the B.E.T. (Brunauer-Emmett-Teller) theory.

The regimes of the various types of gas transport as related to the mean free path (λ) and pore size (d) are found in Table 1. In the viscous regime of gas flow, resistance to
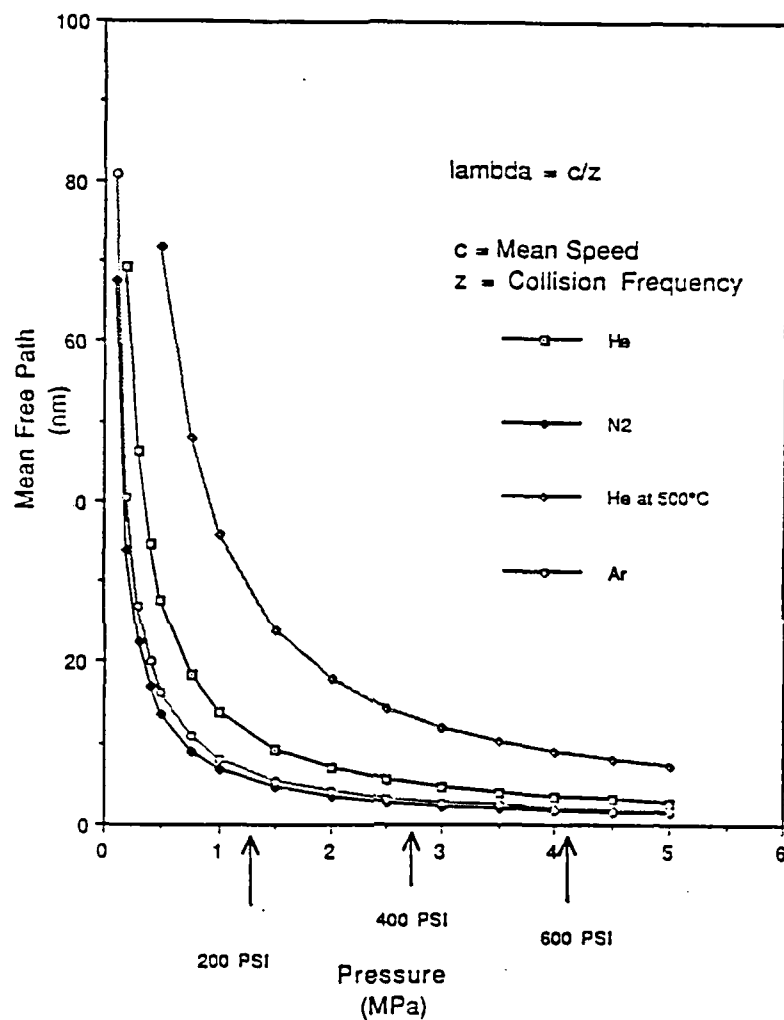
Figure 12. Mean Free Paths of Various Gases as a Function of Pressure.

TABLE 1

Regimes of Gas Flow in Microporous Media [11]

Relation	Mechanism	Restriction to Flow
$\lambda \ll d$	Viscous	Molecule-Molecule Collisions Dominate
$\lambda \cong d$	Slip	Molecule-Wall-Molecule Intermediate
$\lambda \gg d$	Knudsen	Molecule-Wall Collisions Dominate
$d_m{}^* \cong d$	Configurational	

$*$ = molecular diameter

flow is dominated by intermolecular collisions and the velocity profile of the gas flow reaches zero at the wall. One of the fundamental theories applicable to incompressible viscous fluid flow is that of Navier and Stokes [8]. When the velocity of the gas is low throughout the system compared to the speed of sound in the gas, then the flow can be treated as incompressible [12]. Dupuit-Forchheimer assumption is used to obtain the average velocity of the fluid through the pore space relative to the velocity at the surface:

$$v = q/\varepsilon$$

where v is the average pore velocity, q is the velocity at the surface, and ε is the porosity. With the speed of sound in air being approximately 30,000 cm/s, it is safe to assume that flow velocities of less than 10 cm/s can be treated as incompressible even with porosities as low as 10%. For the transpiration of gases at pressures ranging from atmospheric (14.7 psi) to greater than 500 psi, which is the pressure range in which a hypersonic velocity projectile will operate, all three flow mechanisms will exist. During the start of flight the gas flow is expected to be in the Knudsen regime. While in-flight, i.e., during high-pressure range, d and λ are close and hence slip mechanism is likely to dominate. To meet the viscous flow condition, the pore diameter must be much larger than the mean free path of the gas. With mechanical strength already lowered for 100 Å pore diameter porous silica windows, it may not be practical to make rocket windows with pore diameters much larger than about 100 Å for use in practice. Surface flow occurring by surface diffusion is negligible, and hence, was not considered in the discussion.

Figure 13 shows the variation of transpiration flow velocities of helium with pressure through porous silica windows with varying pore diameters. The samples used had radii of 1.2 nm, 5.0 nm, and 8.0 nm, i.e. pore diameters of 24 Å, 100 Å, and 160 Å. These samples were stabilized at 180°C. As the pore diameter increases the transpiration flow velocity increases. This flow velocity varies linearly with pressure within the experimental range.
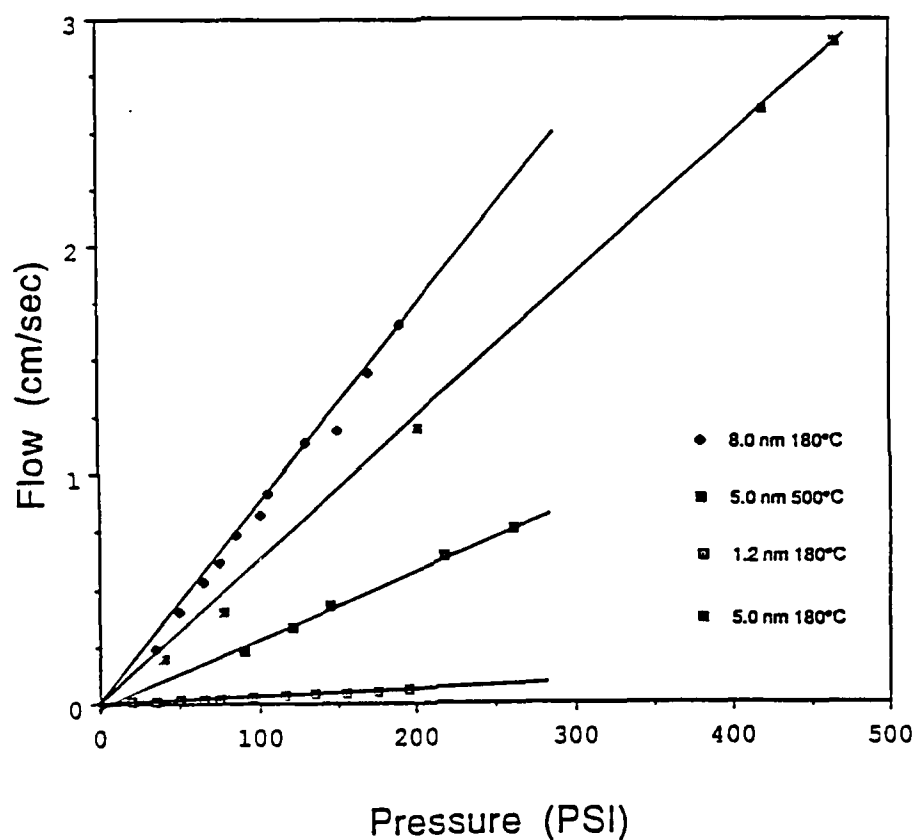
Figure 13. Transpiration Flow Velocity as a Function of Pressure for Various Pore Diameter Porous Silica Windows.

One of the samples of 5.0 nm pore radius was stabilized at 500°C instead of 180°C. Thus, this sample had slightly lower surface area per unit volume and slightly lower specific pore volume, in short a different pore morphology. The transpiration flow rate decrease is very pronounced for such a sample in that the flow velocity declines by 0.67 cm/s to 0.6 cm/s or about 53%. The heat treatment of the porous windows improves its mechanical properties but at the expense of flow rate. Hence, trade-off between mechanical properties and flow properties is essential and requires additional studies.

The thickness of the porous silica windows should not influence the permeability of the diffusing gases. Hence, the permeability values obtained are true permeabilities if and only if they are independent of sample thickness. Figure 14 shows the dependence of permeation flux of helium gas through four different samples of exactly similar pore morphology but different thicknesses ranging from 0.14 to 0.22 cm (see details in Table 2). A constant slope for these data sets, within the error of experimental measurements, indicates that the permeability is indeed true permeability of helium gas for these 100 Å pore diameter porous silica windows. Therefore, a porous rocket window of Type VI silica can be fabricated to given parameters at least within the discussed range of transpiration flow rates.

3.3 Gas Transpiration through Porous Silica Windows

Various gases can be used for transpiration cooling of the rocket windows. The selection criteria for such a gas is essentially based on transpiration flow and cooling characteristics, permitted gas payload weight, absorbance characteristics, and safety during storage, handling, and flight. This part of the research program is still in its early stage because transpiration flow and cooling characteristics were emphasized. The gases considered were He, Ne, Ar, Kr, H_2, N_2, O_2, and CO_2.

The flow properties of some of the gases mentioned above, when they are passed through a 100 Å pore diameter porous silica window, are depicted in Figure 15 as a
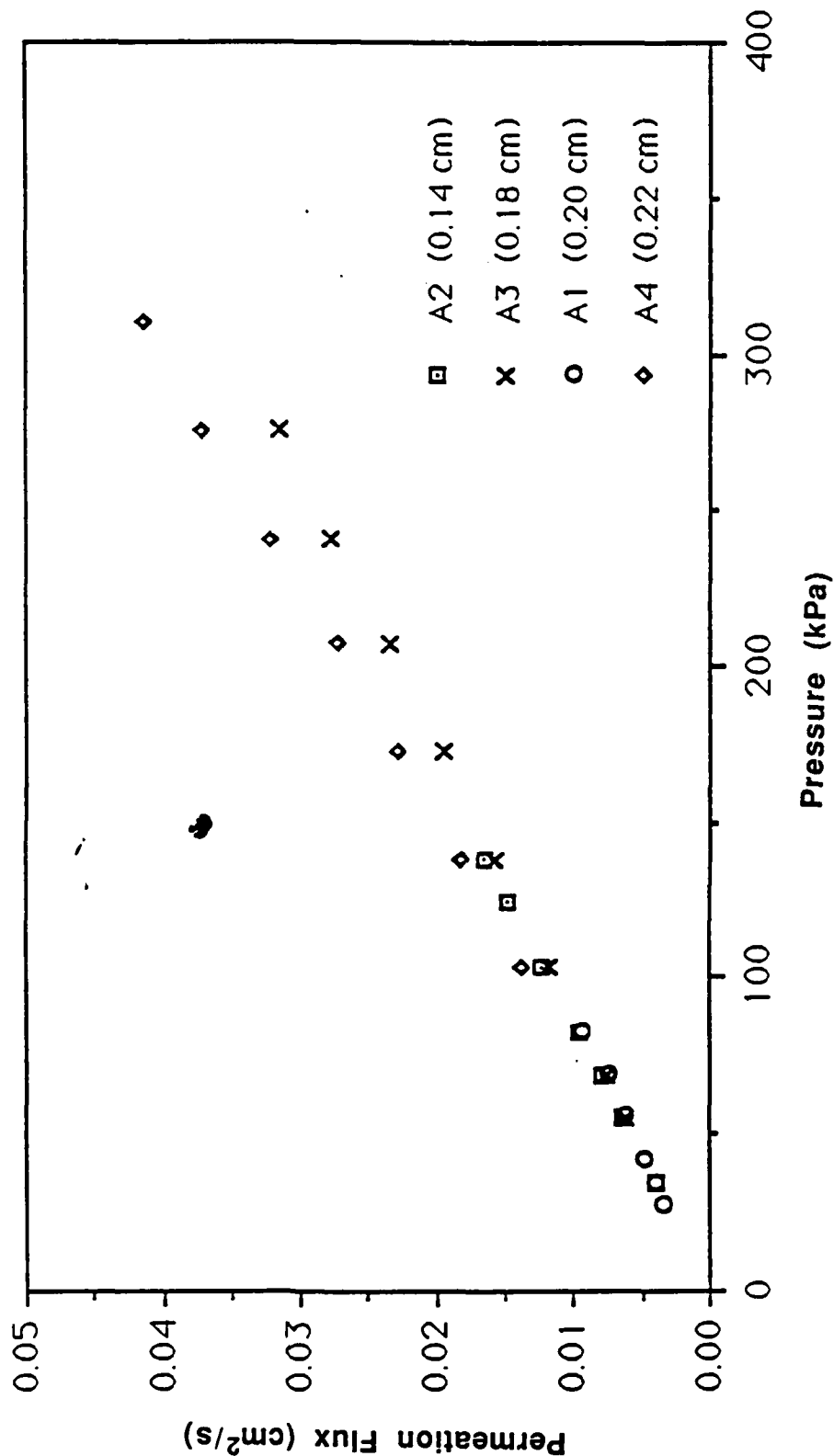
Figure 14. Gas Permeation Flux as a Function of Pressure for Various Thicknesses of the Porous Silica Window.
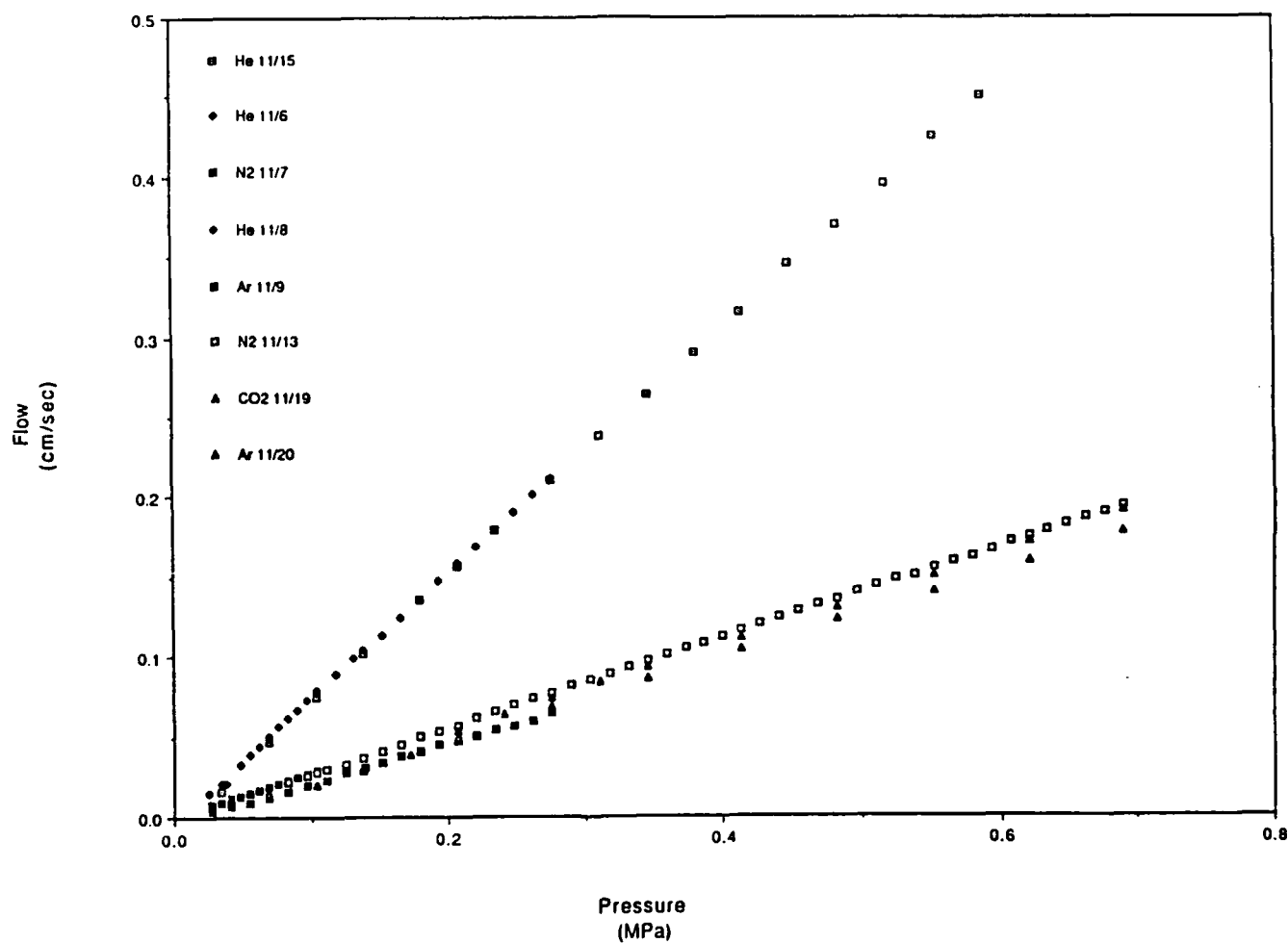
Figure 15. Flow Properties of Various Gases through a 100 Å Pore Diameter Porous Silica Window at Various Pressures.

TABLE 2
Sample Details for Permeability Tests

Details	Sample Designation			
	A1	A2	A3	A4
Area (cm^2)	1.69	1.67	1.72	1.83
Thickness (cm)	0.20	0.14	0.18	0.22
Hydraulic Diameter (Å)	100	108	106	114
Specific Surface Area (m^2/g)	367	356	361	358
Specific Pore Volume (cm^3/g)	0.909	0.955	0.965	1.026
Porosity (%)	66.7	67.8	68.0	69.3
Helium Permeability x 10^4 (cm^2/s kPa)	1.15	1.21	1.15	1.34

function of pressure. A low gas pressure was used. Clearly, the transpiration flow velocity of helium, which has the lowest atomic weight and size (atomic diameter = 0.18 nm), was highest. The flow rate reduces as the molecular weight and size of the gas increases. This is evident by comparing the flow velocity (at constant pressure) data for monatomic gases like helium and argon. For heavier and larger molecular size gases, like N_2 and CO_2 similar lowering of transpiration velocity is observed in Figure 15.

Figure 15 also shows the reproducibility of the results. Here the experiments were repeated for He, Ar, and N_2 on different days. As there was no change in the pore morphology of the porous silica window, the flow characteristics obtained on successive experiments were essentially identical within the limits of experimental error.

The transpiration cooling characteristics are key to the rocket window application. Figures 16 and 17 show the helium transpiration cooling effect at a flow velocity of 0.38 cm/s and 0.52 cm/s respectively. The figures depict the change of both temperature and flow velocity with time. As Figure 16 shows, an initial increase in the flow velocity to a steady-state velocity of 0.38 cm/s results in a temperature drop of about 10°C at the exterior (hot) face of the window to a steady temperature of 46°C. On decreasing this flow rate to zero over a 120 s time period the temperature rises by 25°C to a steady value of 71°C. The situation was somewhat reversed in the next experiment wherein the steady flow was interrupted completely for 120 s time intervals. Figure 17 shows a starting steady-state flow velocity of 0.52 cm/s at which the exterior face of the window was at 116°C. On reducing this flow velocity to zero for 120 s, this temperature soared to about 160°C thereby showing a 44°C rise. On gradual return to the original flow velocity the temperature declined to 116°C, the starting value. The experiments were repeated and the results obtained were reproducible. Clearly, at higher flow rates the cooling effects will be more pronounced. Also, as the thermal boundary layer is shifted to a greater distance from the window surface, a more dramatic cooling effect is expected. Obviously, more experimentation is warranted in order to monitor this effect for the rocket window application.

Figure 16. Temperature and Transpiration Flow Velocity of 0.38 cm/s as a Function of Time.

Figure 17. Temperature and Transpiration Flow Velocity of 0.52 cm/s as a Function of Time.

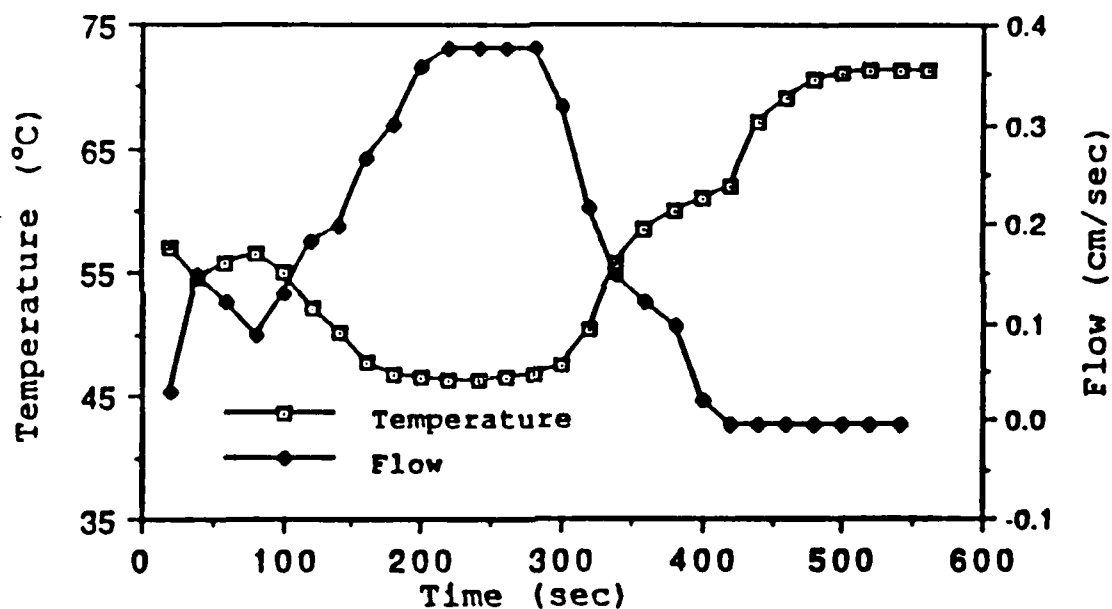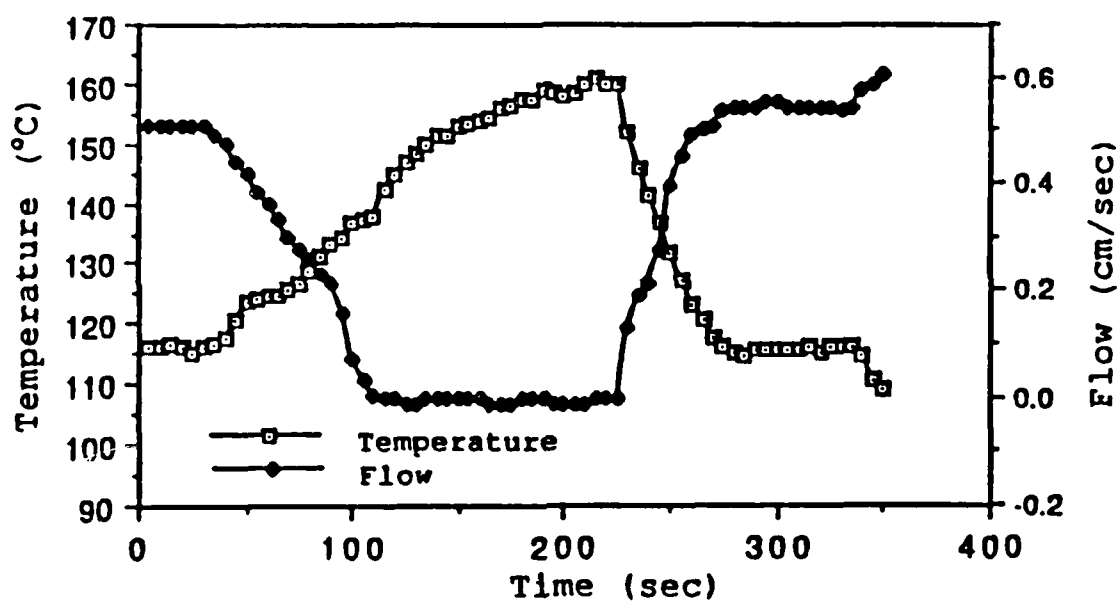The variation of the permeation flux of various gases through a 100 Å pore diameter porous silica window with pressure is shown in Figure 18. At pressures like 0.125 MPa and lower, each of the gases have a linear rate of increase of flux with pressure. A linear graph is also indicative of a constant permeability. From previous results we know that this permeability is actually "true" permeability. It is evident that as the atomic weight of the noble gas increases its permeation flux and its permeability (slope of the line) decreases with increasing pressure. For diatomic gases like H_2, N_2, and O_2 a similar conclusion can be made, as seen from Figure 18. Figure 19 shows the permeability of various gases as a function of pressure, including higher pressures (up to 400 psi). The values of permeabilities are almost constant as a function of pressure within the given range, as expected. The permeabilities resulting from viscous flow have a linear dependence on pressure while that resulting from Knudsen flow have no dependence at all [8]. Hence, the conditions of testing here indicate Knudsen diffusion as the predominant mass transport mechanism [13].

In Knudsen diffusion theory, permeabilities of gases vary linearly with the inverse square root of the molecular weight of the gas due to the dependence of the mean free path of gas molecules on their average velocity. To confirm the dominant mechanism of mass transport (diffusion) the permeabilities of various gases obtained using sample A1 were plotted against the inverse of the square root of their molecular weight. A straight line approximation suggests Knudsen flow in the tested samples under the given condition as shown in Figure 20.

3.4 High-Temperature Spectroscopy through Porous Silica Windows

Two different setups were tried in order to study the effects of high temperatures on UV transmirsion of porous silica windows.

One setup used external heating by an oxygen-acetylene flame with a wavelength shifter detector. Fluorescence activity was observed in the detector at temperatures around that of the oxygen-acetylene flame. This wavelength shifter detector absorbed UV
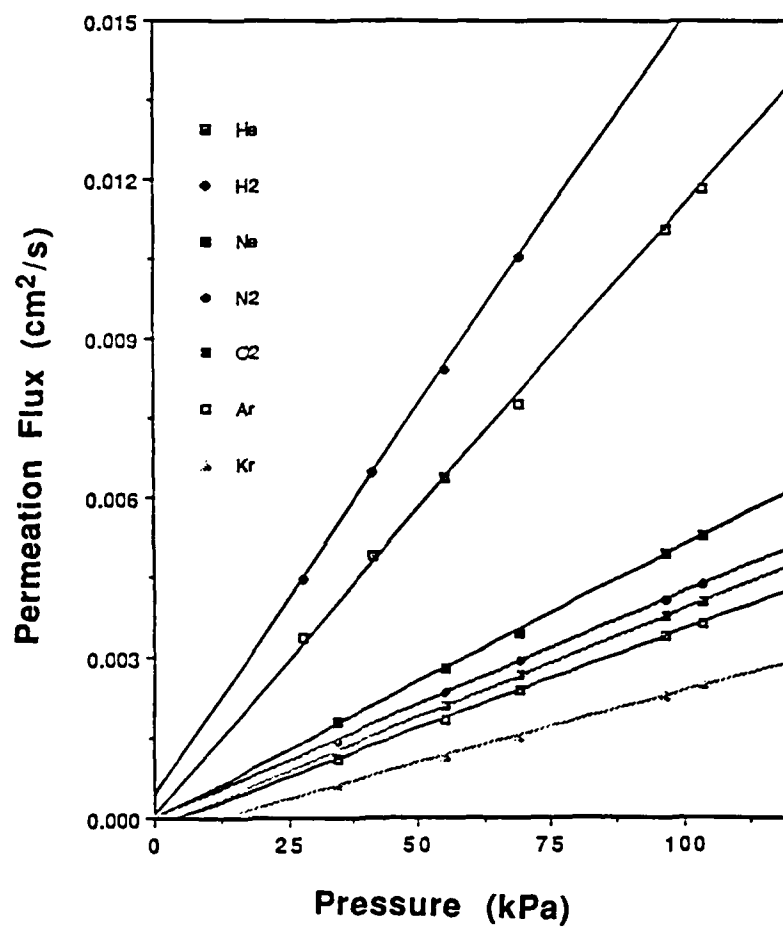
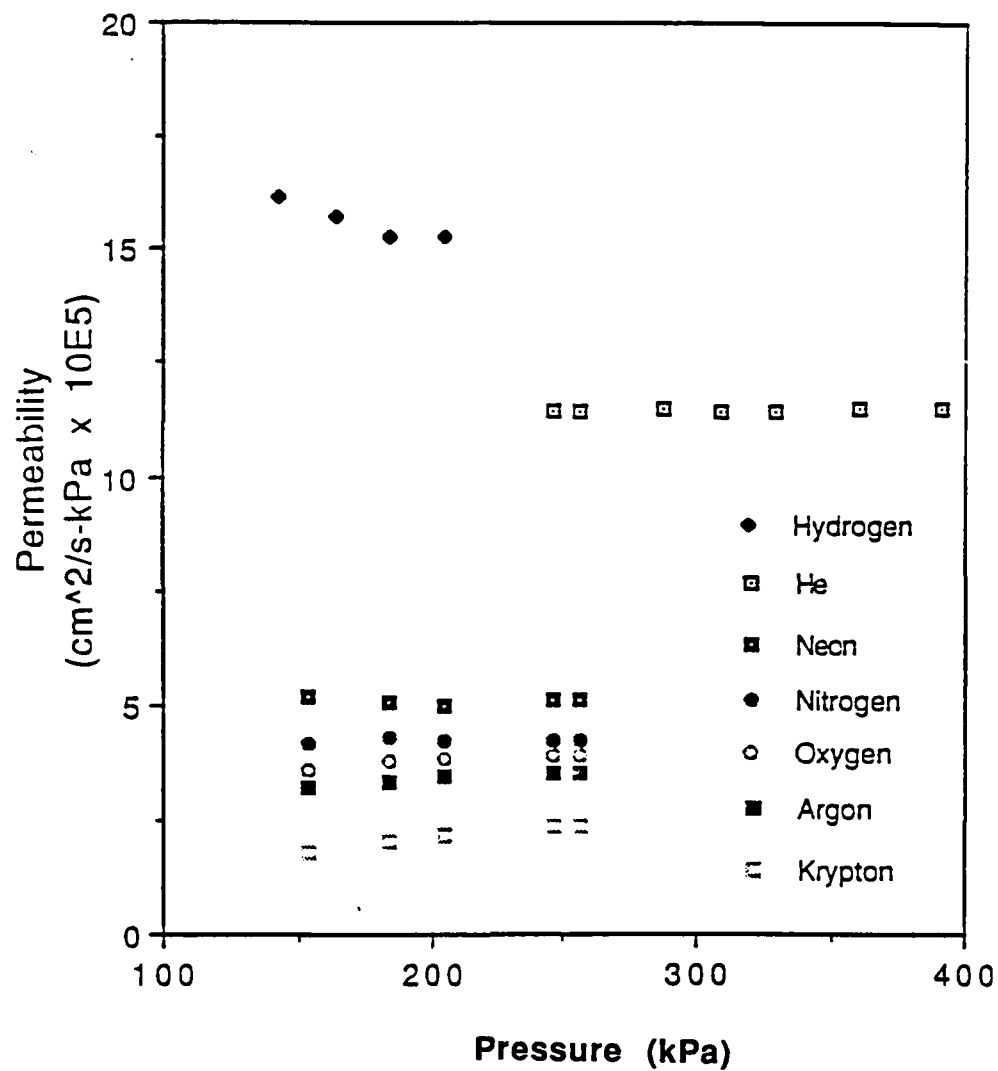**Figure 18. Variation of Permeation Flux of Various Gases with Pressure**

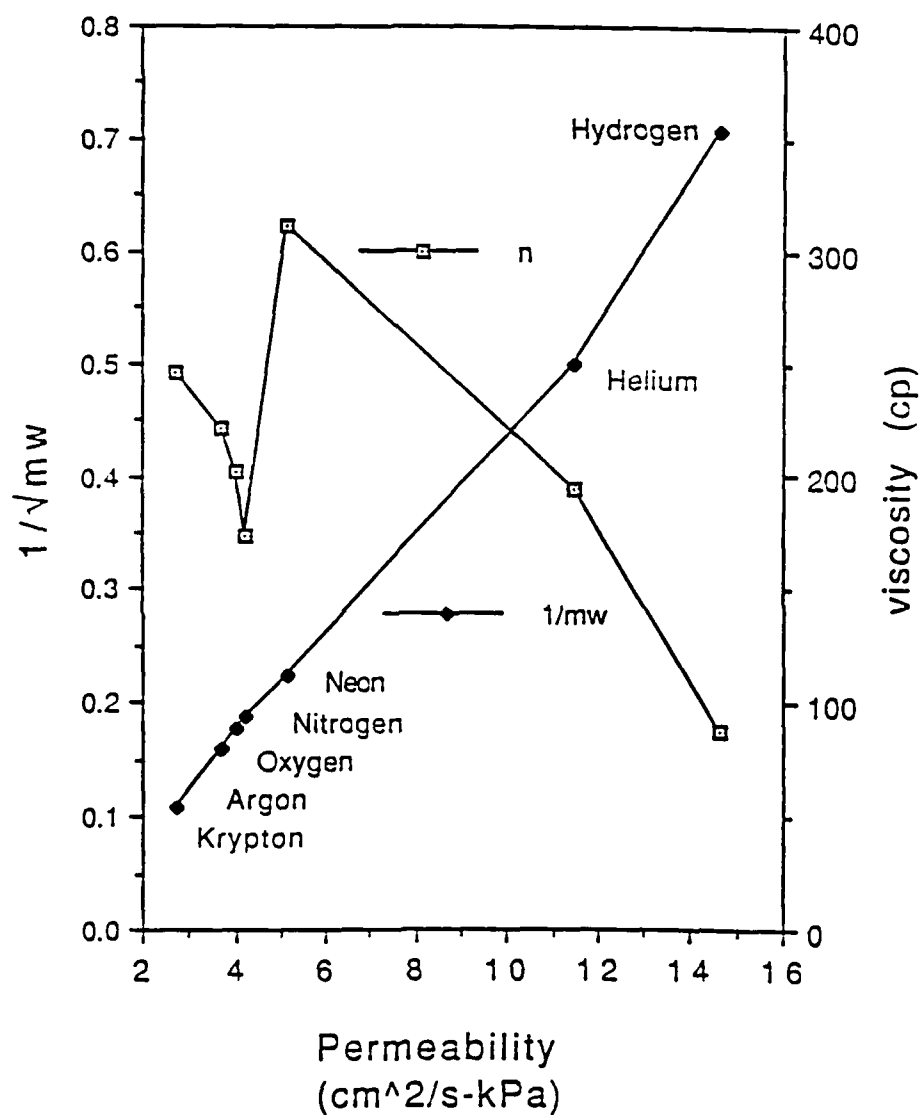**Figure 19. Permeability of Various Gases as a Function of Pressure.**

Figure 20. Variation of Permeability with Inverse Square Root of Molecular Weight and Viscosity of Various Gases.

radiation and emitted radiation of ~600 nm wavelength. Thus, the results of this test were indicative of UV transmission, but they were not quantifiable.

A conventional furnace was utilized along with modifications in the analysis chamber of a spectrophotometer. Figures 21 through 29 show the transmittance spectra through porous silica windows with 25, 50, and 112 Å pore diameters at temperatures of 25°C and 400°C (averaged). The full-range transmission characteristics at room temperature (25°C) are shown in Figures 21 through 23. Note the strong absorption due to free H_2O and chemically held surface hydroxyls (actually silanol groups). The full-range transmission characteristics at 400°C (averaged) for the above samples are shown in Figures 24 through 26. On comparing the 25°C transmittance characteristics with those at 400°C it was found that the transmittance was enhanced, irrespective of the pore size. This increased transmittance as ascribed to the removal of moisture (free water) in the pores of the stabilized gels. Also, the number of silanols were reduced drastically at that temperature. This resulted in a lowering of the intensities of the peaks due to the silanols.

The ultraviolet cutoff was chosen arbitrarily at 5.0% transmittance. The comparison of low wavelength range scans for silica windows of 25, 50, and 112 Å pore diameters are shown in Figures 27, 28, and 29, respectively. As is clear from Figure 27, the UV cutoff wavelength for 25 Å pore diameter porous silica window was lowered by 15 ± 5 nm at 400°C compared to that at 25°C. Hence, the increase in temperature actually enhanced the transmittance characteristics by slightly broadening the spectrum into the UV range. This phenomenon, though reproducible for 25 Å pore diameter samples, did not appear to occur for 50 Å and 112 Å pore diameter porous silica windows, as is evident from Figures 28 and 29.

This observation immediately leads to the mechanisms wherein subtle effects are induced by the varion in pore diameters in porous silica [14]. Rayleigh scattering from particles requires that the particles be at least one-tenth the size of incident wavelength. Secondly, the particles must have an effective index of refraction slightly
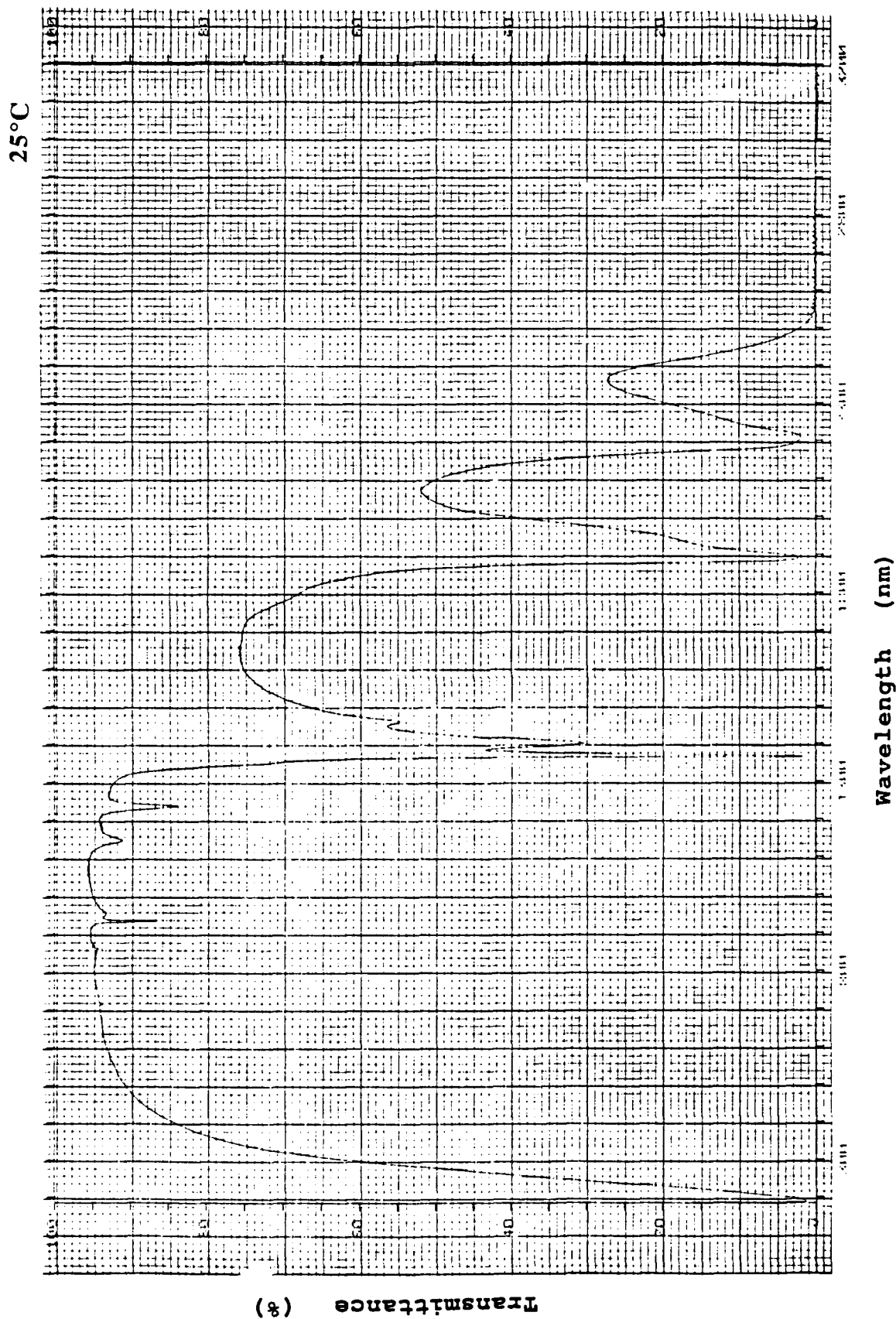
Figure 21. Transmittance Characteristics at 25°C Through a Porous Window with 25 Å Pore Diameter.
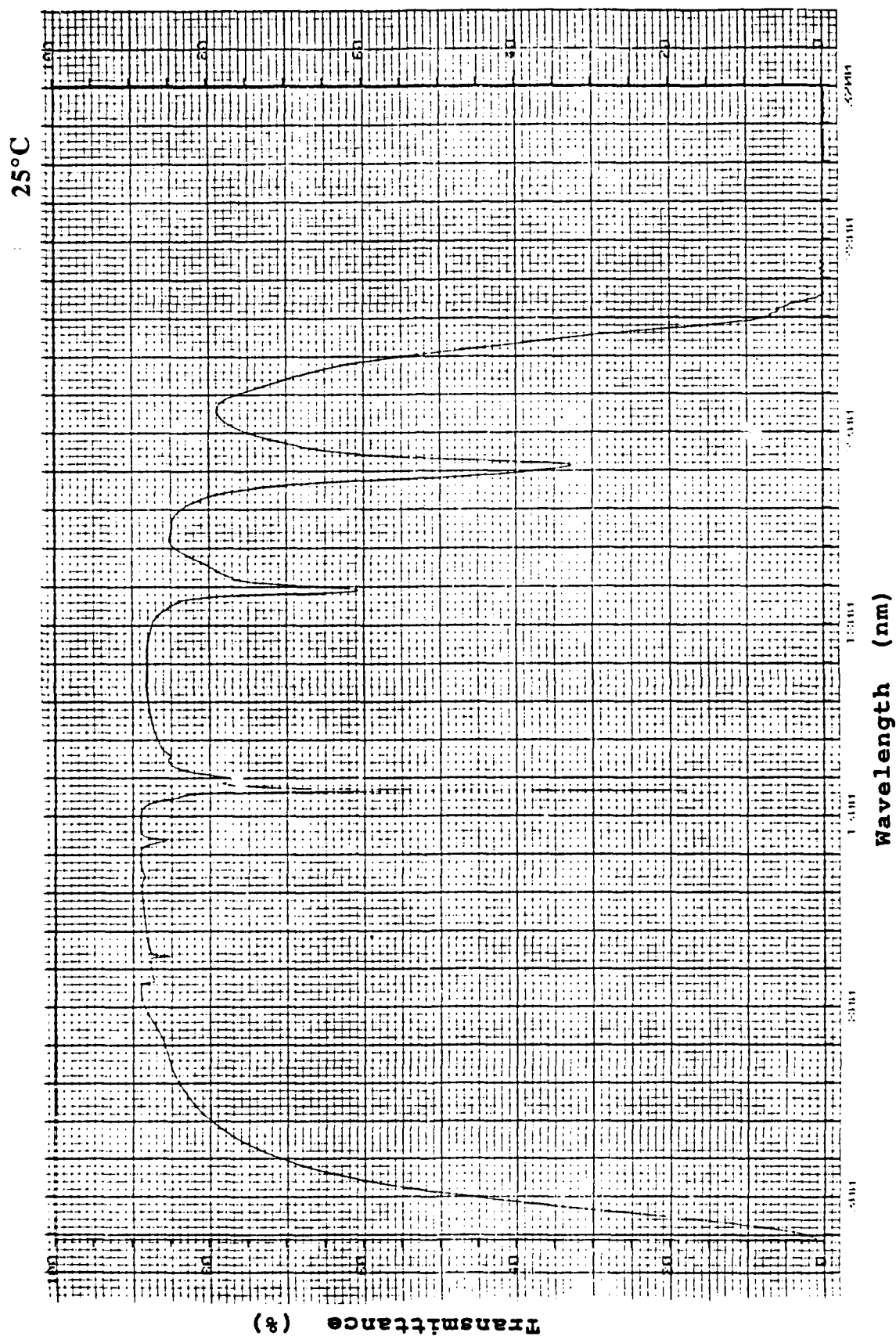
Figure 22.Transmittance Characteristics at 25°C Through a Porous Window with 50 Å Pore Diameter.
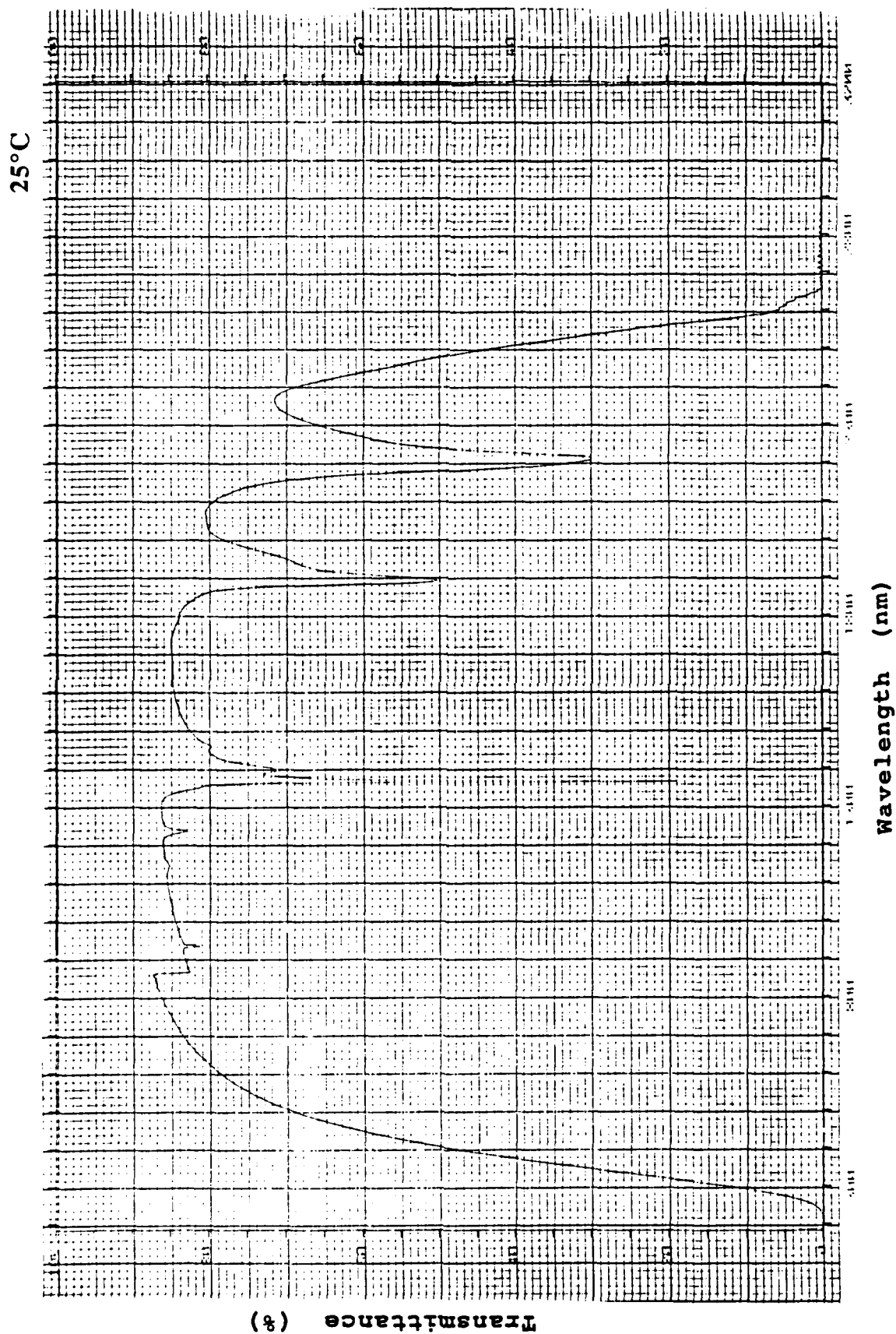
Figure 23. Transmittance Characteristics at 25°C Through a Porous Window with 112 Å Pore Diameter.
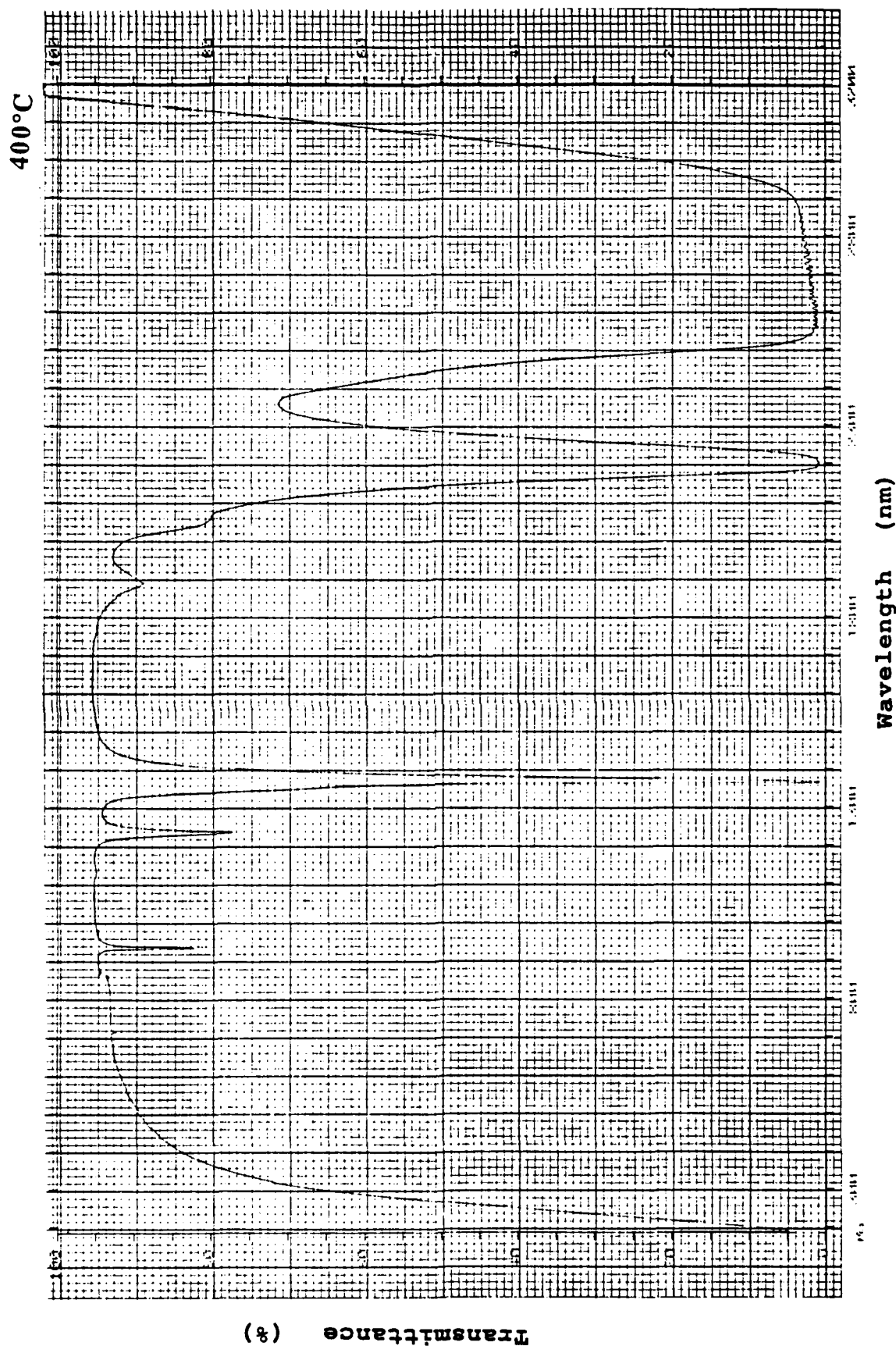
Figure 24. Transmittance Characteristics at 400°C Through a Porous Window with 25 Å Pore Diameter.
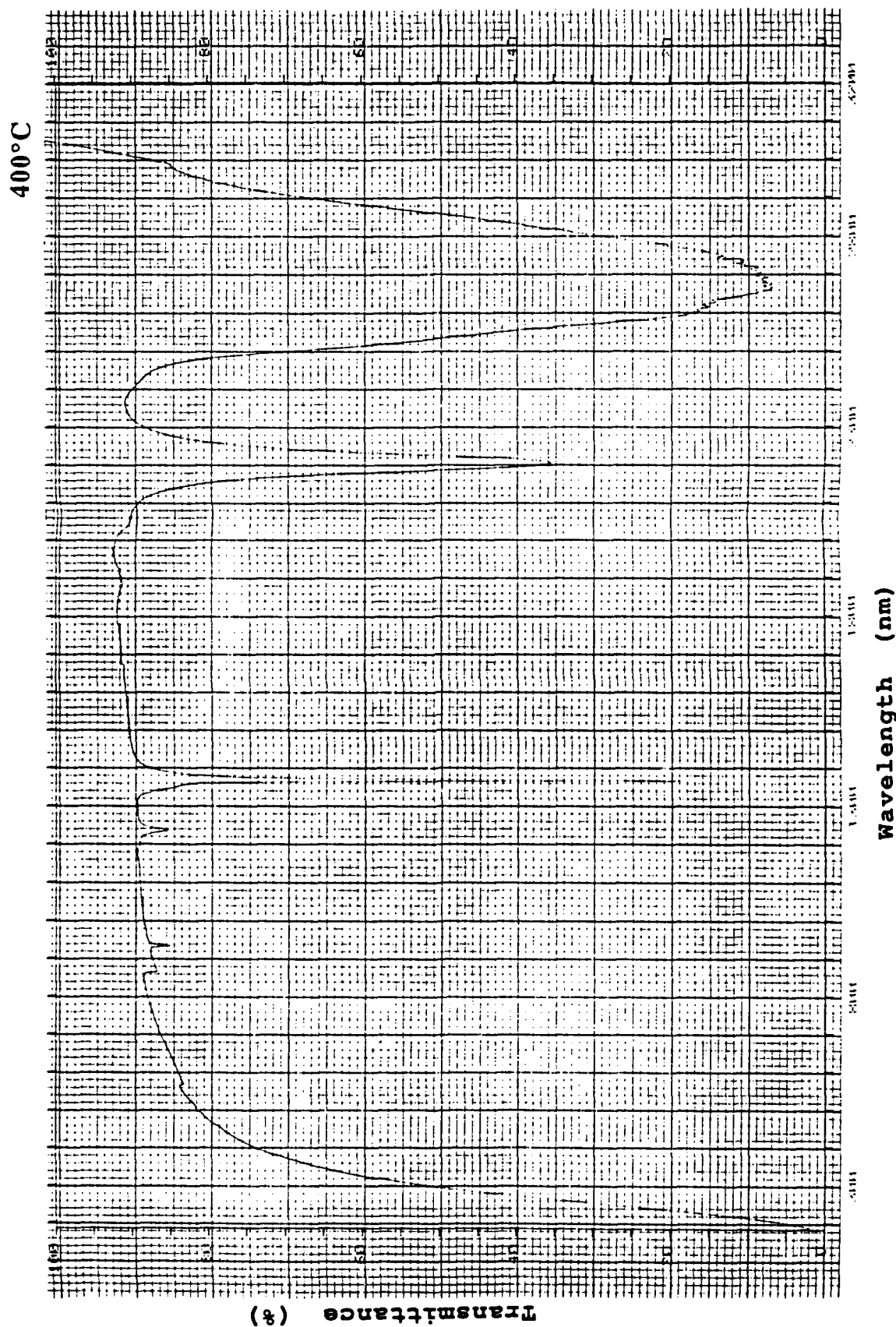
Figure 25. Transmittance Characteristics at 400°C Through a Porous Window with 50 Å Pore Diameter.

Figure 26. Transmittance Characteristics at 400°C Through a Porous Window with 112 Å Pore Diameter.

Figure 27.Comparison of Transmittance Characteristics at 25°C and 400°C Through a Porous Silica Window with 25 Å Pore Diameter.
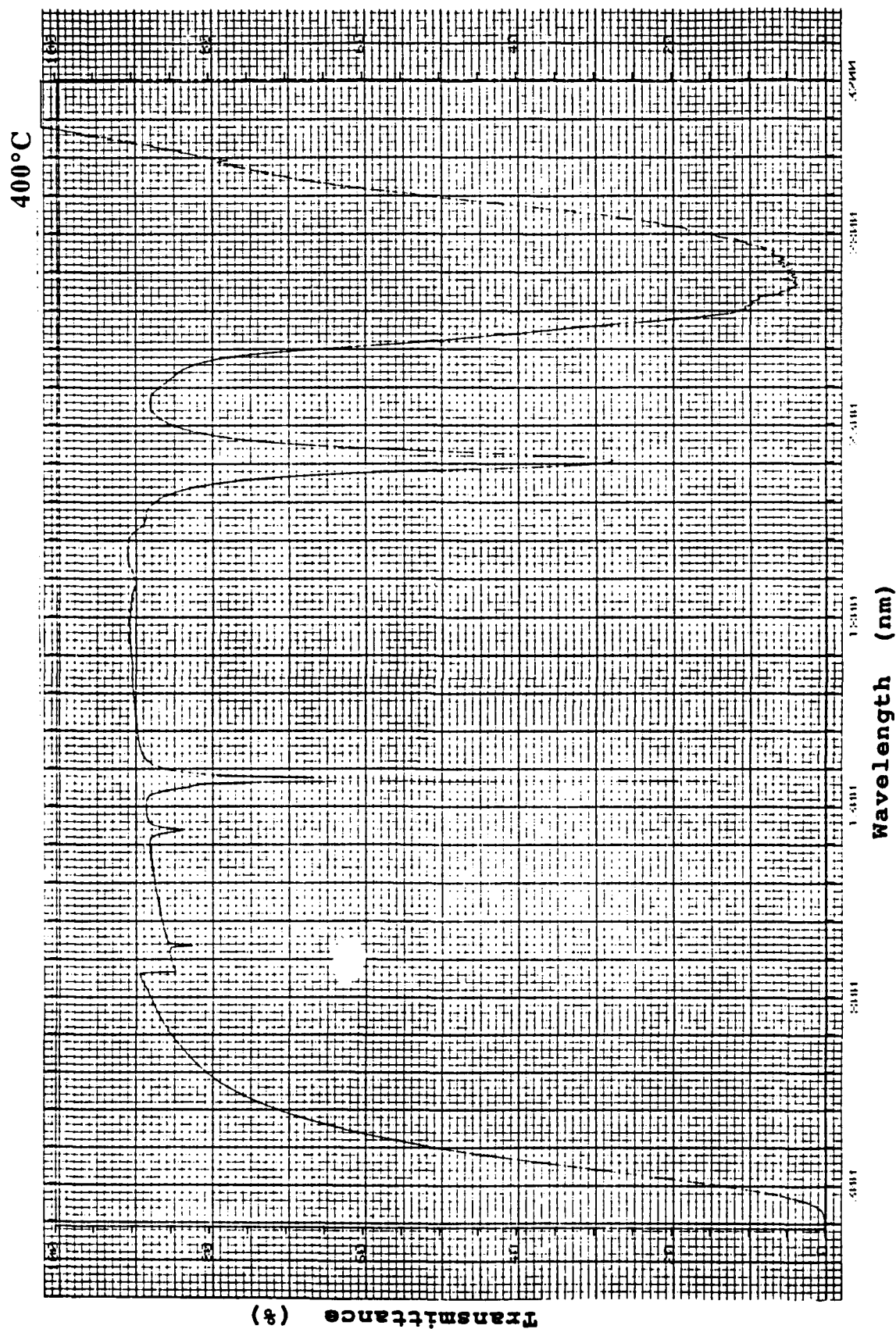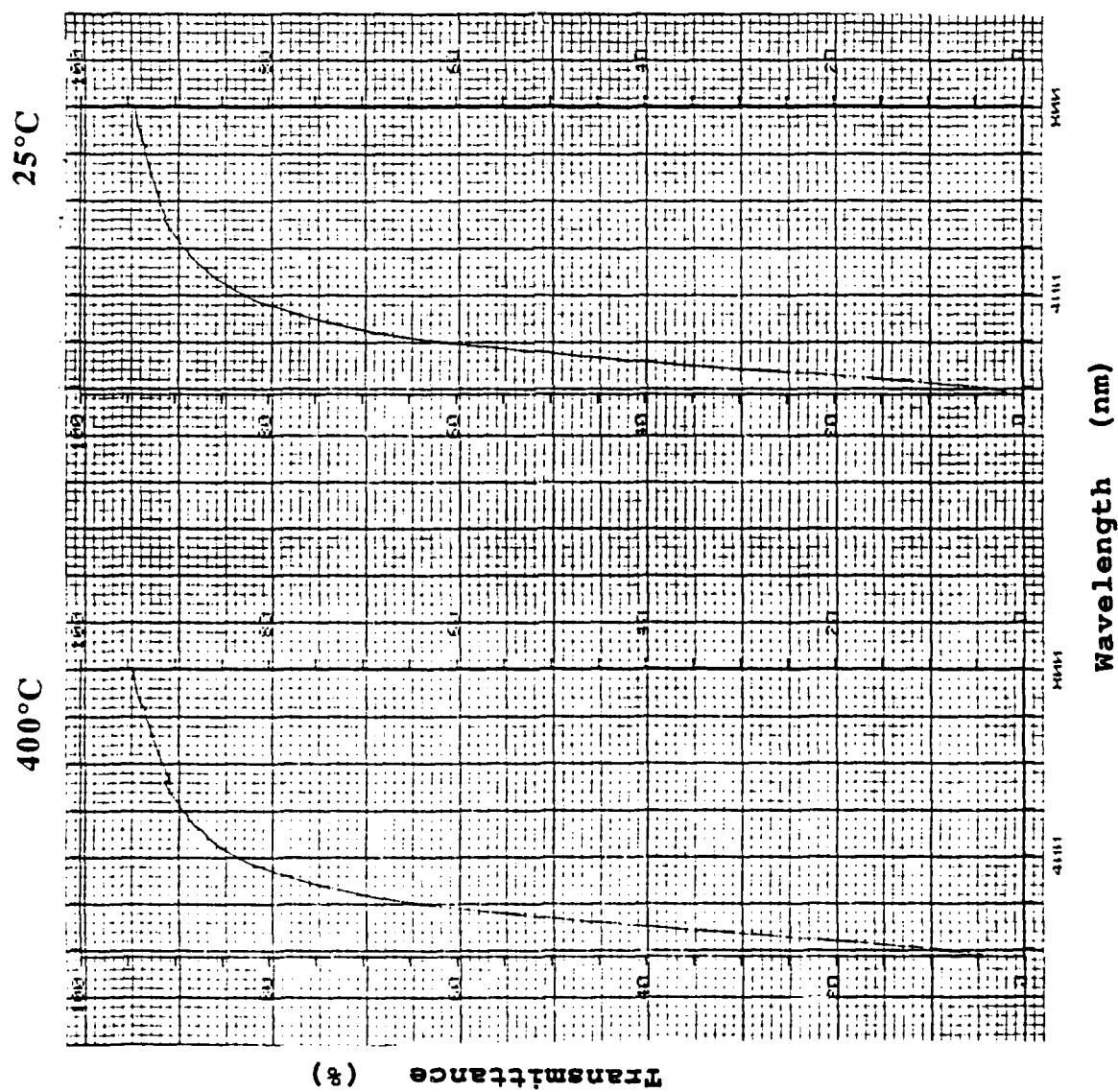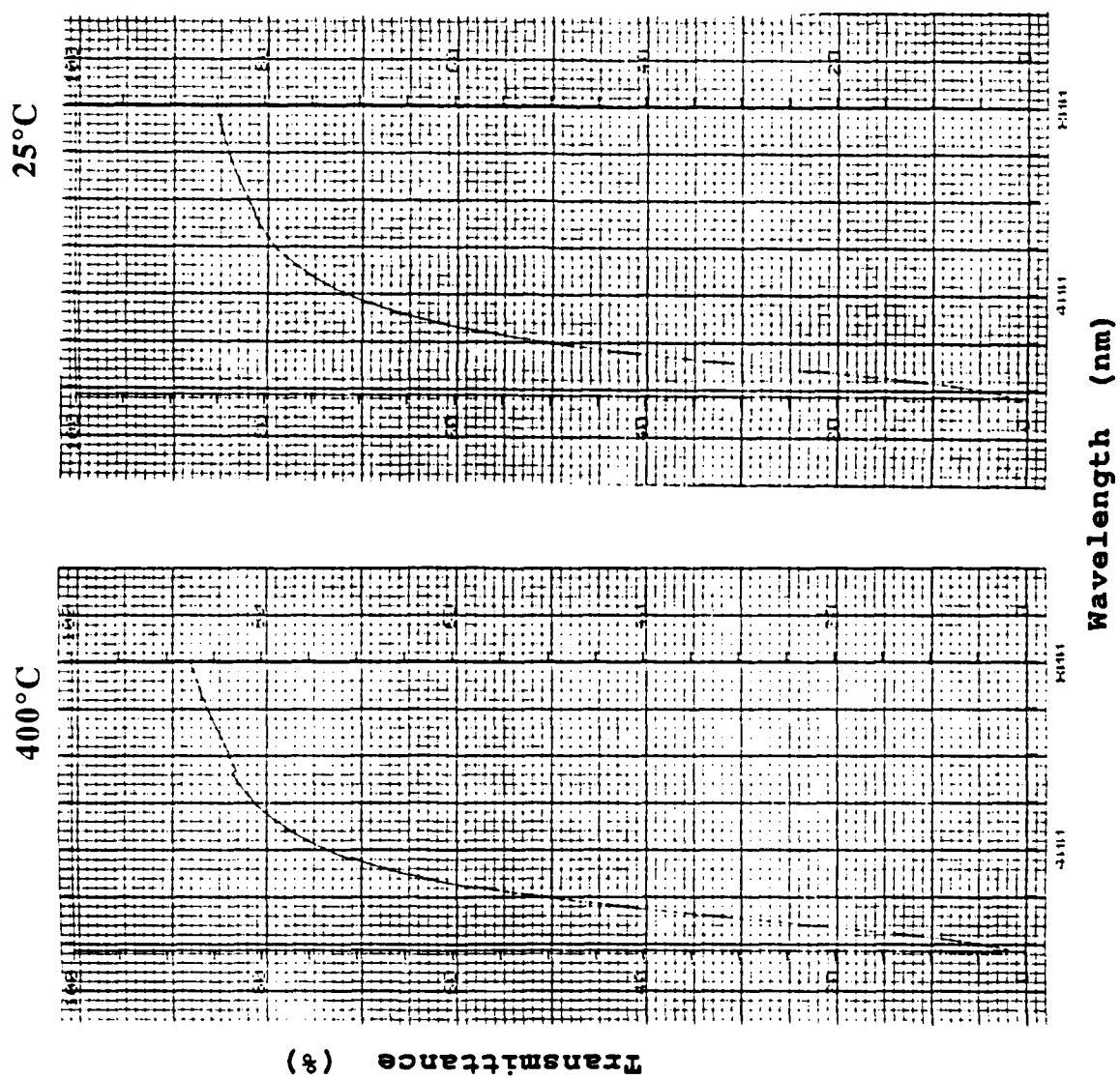
Figure 28. Comparison of Transmittance Characteristics at 25°C and 400°C Through a Porous Silica Window with 50 Å Pore Diameter.
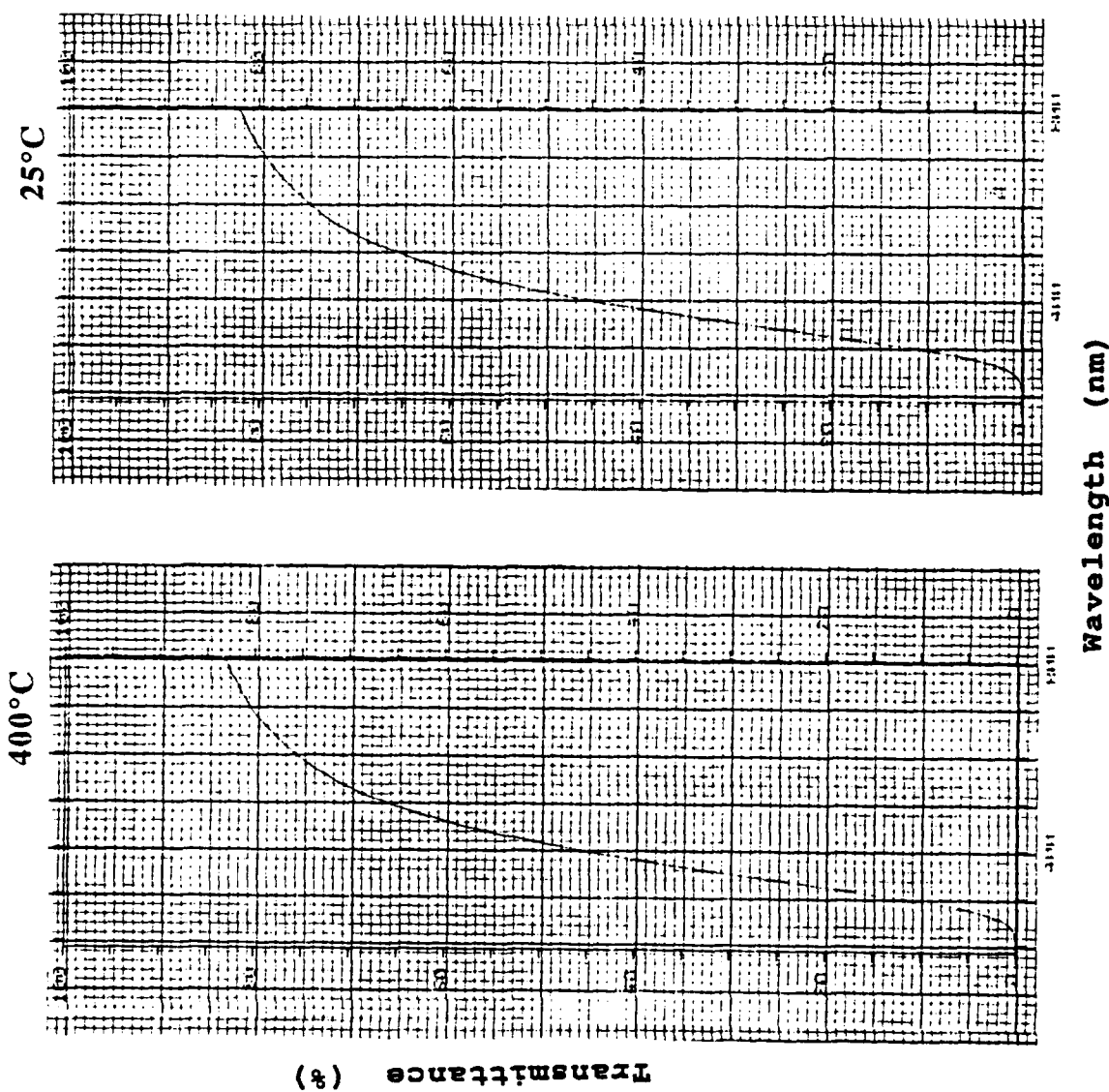
Figure 29. Comparison of Transmittance Characteristics at 25°C and 400°C Through a Porous Silica Window with 112 Å Pore Diameter.

higher than the surrounding medium. Based on the assumption that the index of refraction of pore surface is greater than that of air and that the particle size was found (estimated by a close packing model) in the right size range. A close match between the theoretical and experimental results was obtained [14].

Microscopically, however, the mechanism for UV cutoff wavelength dependency can be described in terms of cyclotrisiloxane, D_2 and cyclotetrasiloxane, D_1 rings [15]. The D_1 ring is a four-membered siloxane ring with characteristic "defect" peak at 605 cm^{-1}. The D_2 ring is a three-membered siloxane ring with characteristic "defect" peak at 495 cm^{-1}. The number of rings present is however low and concentrated only at the pore surface. The highly strained three-member D_2 ring is easier to form in a small pore than a large pore. The D_1 should form with greater ease in a large pore. The mechanism of formation of the D_1 ring involves condensation of surface silanol adjacent to the D_2 ring, which in effect reduces the concentration of surface silanols, thus affecting the UV cutoff wavelength directly. In fact, calculations done by West et al. [16] using intermediate neglect of differential overlap (INDO) molecular orbital model suggest that increased concentrations of surface hydroxyls tend to shift the UV cutoff to higher wavelengths. A similar effect is observed on reducing the temperature. These calculations support the observations made in the experiments conducted during this research. The concept of activation energy for the removal of surface hydroxyls is currently under development [17]. A more in-depth study of temperature effects on the UV cutoff is warranted.

3.5 Thermal Stability and Shock Resistance of Porous Silica Windows

Thermal stability of silica gel monoliths was first tested using dilatometry in order to define temperature range for application of the gels [18]. Zhu et al. [19] further studied the hysteretic behavior in a dilatometric study and related the bulk behavior to microscopic mechanism. Previous work on porous silica that has been derived via sol-gel processing indicates that as the pore diameter increases the mean linear coefficient

of thermal expansion (CTE) first increases and then decreases. The maximum in this curve was for a pore 134 Å in diameter [14], which in reality is the pore size for minimum expansion of porous silica (CTE = 0.38 ppm/°C). This information helped in defining the region of optimum stability of the window. A porous silica window with a pore diameter of 110 Å yields a CTE of 0.5 ppm/°C. To obtain a porous silica window with a CTE of 0.5 ppm/°C or less the pore diameter may range from 100 to 170 Å. In this research the maximum (average) pore diameters were kept within the above stated range.

Some dilatometry studies have shown that the pore structure of stabilized gels (about 800°C) does not change at all up to 400°C. Exposure to higher temperatures and very long duration may change the pore structure, which would alter the transpiration rate of the gases flowing through it. However, thermal mechanical analysis (TMA) on silica gel has shown that its shrinkage after stabilization is almost negligible until 700°C [5]. Hence, the temperature tolerated by porous silica windows is extremely high. It should be pointed out that by tailoring the ultrastructure of these porous silica windows this temperature may be enhanced.

Thermal shock testing essentially evaluates the resistance of the material to extreme variation in temperatures. For a rocket window the normal storage and handling temperatures would be limited to MIL-SPEC temperature range (-55°C to +125°C). It is during deployment that the projectile is expected to come across extreme variations in temperatures. The samples were tested in accordance with ASTM C149-86. The temperature range extended from -77°C to +500°C.

Not a single sample of any of the pores sizes cracked during the quenching process. This indicated the extremely good thermal shock resistance of the porous silica windows. This excellent behavior is ascribed to the inherently excellent thermal shock resistance property of silica and the interconnectivity of the structure in the porous window, which is a three-dimensional random network. Hence, porous silica windows for transpiration cooling of rocket windows are desirable from thermal shock resistance

criterion.

3.6 Mechanical Properties of Porous Silica Windows

The mechanical properties of the rocket windows are important as they are an integral part of the rocket guidance system. The surface microhardness using Vicker's indenter and impact strength using ASTM C368-77 (reapproved 1982) were the major tests carried out.

It is known that porous silica is a brittle material and the nature of its failure is catastrophic. The strength factor, S, was calculated by using:

$$S=I/t^2$$

where,

    I = average impact for fracture
and,
    t = average thickness at the point of impact

Figure 30 shows the variation of Vicker's hardness and hydroxyl concentration as a function of processing temperature. By 900°C the Vicker's hardness is considerably high and the concentration of hydroxyls is low. This information was utilized in choosing the processing temperature for stabilization. Literature regarding the mechanical properties of porous sol-gel silica monoliths is almost nonexistent [20].

Table 3 compares the mechanical properties of porous silica windows. In general, as the pore diameter increases the mechanical properties of the porous silica window deteriorate. For example, a pore diameter change from 25 to 50 Å leads to a lower impact of fracture from 1.36 to 0.952 J, or a reduction of 30%. The Vicker's hardness shows trends similar to those of impact of fracture. For instance, a pore diameter change from 25 to 50 Å leads to a lower Vicker's hardness from 74.0 to 50.0 kg/mm^2,
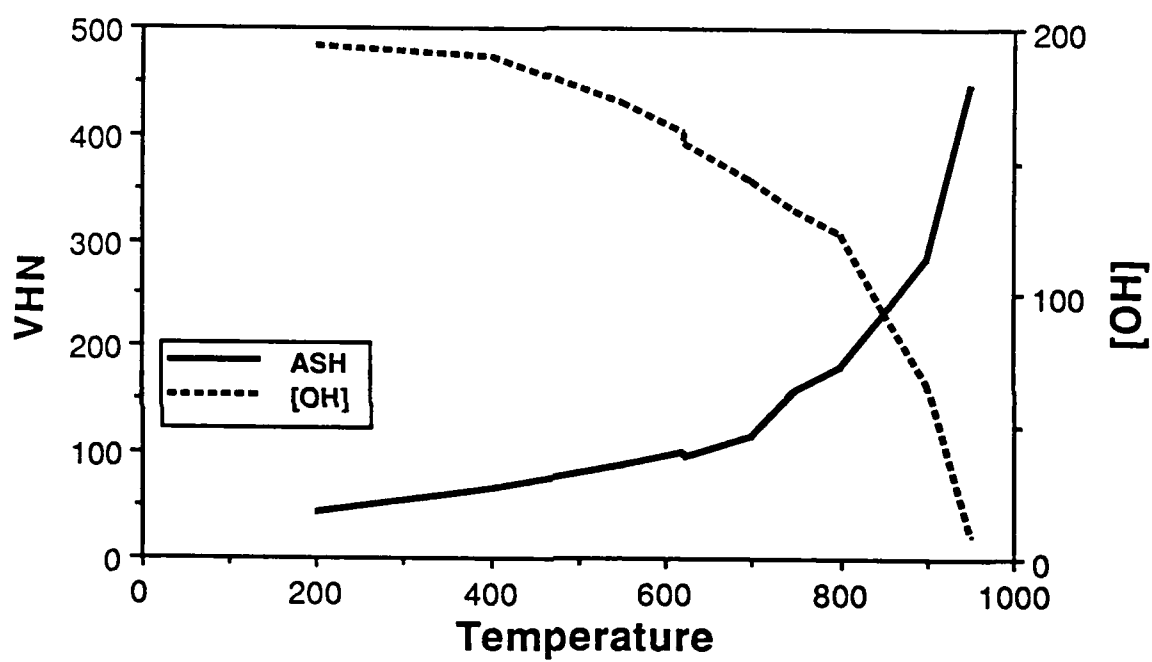
Figure 30. Change in Sample Microhardness and OH- Concentration with Temperature.

TABLE 3

Comparison of Mechanical Properties of Porous Silica Windows

Property	Pore Diameter of Porous Silica Window		
	25 Å	50 Å	112 Å
Impact of Fracture (J)	1.36	0.952	0.408
Vicker's Hardness Number (kg/mm^2)	74.0	50.0	18.0
Strength Factor (MPa)	0.83	0.44	0.06

or a reduction of 33%. The calculated strength factors show decreasing values as the pore size increases. A pore diameter change from 25 to 50 Å reduces the strength factor from 0.83 to 0.44 MPa, a reduction of 47%.

As is evident from the above discussion, an increase in the pore size degrades the mechanical integrity of the window. However, the porosity is essential for the windows to permit transpiration. With these conflicting requirements an optimization in transpiration rate and mechanical strength is essential, which warrants further research. It should be noted from gas diffusion and transpiration studies that the measured permeability is "true" permeability which will not change with increased thickness of the porous media. Hence, thicker windows, which will have higher mechanical strength, can be obtained without sacrificing transpiration properties of the gas. Hence, the likelihood of obtaining the stated transpiration windows optimized for transpiration rate and mechanical strength is very high.

4. CONCLUSIONS

This research effort has successfully developed transpiration-cooled porous silica windows for rocket guidance systems. The research establishes the viability of the novel concept of cooling by transpiration. Sol-gel technology was utilized for the fabrication of porous silica windows of various pore diameters. Various gases were utilized and their diffusion and transpiration properties studied. For a transpiration velocity of 0.52 cm/s of helium, a 44°C temperature drop was observed. High-temperature spectroscopy showed improved transmittance characteristics of porous windows, especially with 25 Å pore diameter. The thermal stability and thermal shock resistance of these porous silica windows were excellent, irrespective of the pore diameters. The mechanical properties of the porous windows deteriorated with increasing pore diameter. Though, the mechanical properties of windows with pore diameters of about 100 Å were reasonable. It was noted that the gas permeability was indeed "true" permeability and thus, *the thickness of the window will not affect the* transpiration behavior of the gas. Therefore, thicker windows can be made which will offer much higher mechanical resistance without sacrificing the gas transpiration through them for cooling. Such optimization is definitely possible after further research. Also, these rocket windows could be manufactured at a fraction of the cost of the currently used materials.

5. REFERENCES

1. J.D. Anderson, pp. 125 in *Introduction to Flight*, 3rd Ed., McGraw-Hill Book Company, New York, NY, 1989.

2. J.L. Threlkeld, pp. 138-140 in *Thermal Environmental Engineering*, 2nd Ed., Prentice-Hall, Englewood Cliffs, NJ, 1970.

3. I. Matsuyama, K. Susa, S. Satoh, and T. Suganuma, *Bulletin of the American Ceramic Society*, **63** [11] 1408-1411 (1984).

4. J. Phalippou, T. Woignier, and J. Zarzycki, pp. 70-87 in *Ultrastructure Processing of Ceramics, Glasses, and Composites*. L.L. Hench and D.R. Ulrich, eds., John Wiley & Sons, NY, 1984.

5. J.L. Noguès and W.V. Moreshead, "Porous Gel-Silica, A Matrix for Optically Active Components," *J. Non-Crystalline Solids*, **121** 136-142 (1990).

6. L.L. Hench and A. Fozmoe, "Multifunctional Silica Optics," *Materials Research Society Symposium Proceedings*, **175** 23-24 (1989).

7. J. Frankel, "Viscous Flow of Crystalline Bodies Under the Action of Surface Tension," *J. Phys. (Moscow)*, **9** [5] 385-391 (1945).

8. A.E. Scheidegger, *The Physics of Flow Through Porous Media*, University of Toronto Press, Toronto, Canada, 1974.

9. A. Fozmoe and L.L. Hench, "Transpiration Cooled Porous Type VI Rocket Windows," *Materials Research Society Symposium Proceedings*, **180** 843-848 (1990).

10. P.W. Atkins; pp. 653 in *Physical Chemistry*, W.H. Freeman and Co., New York, NY, 1986.

11. R.E. Cunningham and R.J. Williams, *Diffusion in Gases and Porous Media*, Plenum Press, New York, NY, 1980.

12. D.J. Tritton; *Physical Fluid Dynamics*, Clarendon Press, New York, NY, 1988.

13. A. Fozmoe and L.L. Hench, "Gas Permeability in Porous Gel-Silica," *Conference on Ultrastructure Processing of Ceramics, Glasses, and Composites,*

Feb. 18-21, 1991, Orlando, FL.

14. E.A. Elias, "Pore Size Effects on the Thermal Stability of Sol-Gel Derived Silica Monoliths," *M.S. Thesis*, University of Florida, Gainesville, FL, 1989.

15. L.L. Hench and J.K. West, "The Sol-Gel Process," *Chem. Rev.*, **90** 33-72 (1990).

16. J.K. West, S. Wallace, L.L. Hench, and C.R. Lishawa, "Quantum Calculations on Silica Structures," *Proceedings of 4th Ultrastructure Processing of Ceramics, Glasses and Composites*, Tucson, AZ, 1989.

17. J.K. West and S. Wallace; private communication.

18. F. Wang, "Thermal Stability of the Porous Gel-Silica," *M.S. Thesis*, University of Florida, Gainesville, FL, 1988.

19. B.F. Zhu, G.F. Wang, and L.L. Hench, "Dilatometry of Silica Gels," *Proceedings of 4th Ultrastructure Processing of Ceramics, Glasses and Composites*, Tucson, AZ, 1989.

20. S.C. Park and L.L. Hench, "Physical Properties of Partially Densified SiO_2 Gels," pp. 168-172 in *Science of Ceramic Chemical Processing*. Edited by L.L. Hench and D.R. Ulrich, John Wiley and Sons, New York, NY, 1986.

APPENDIX A

Gas Permeability in Porous Gel-Silica

Albert Fosmoe II and Larry L. Hench

Advanced Materials Research Center

University of Florida

Alachua, Florida 32615

INTRODUCTION

It has been previously proposed that the ultraporous structure of sol-gel derived Type VI silica can be used and modified advantageously for rocket window applications [1,2]. The need for better optically transparent windows in the guidance system of hypersonic (Mach > 5) rockets results from the intense thermal boundary layer created by a rocket under high Mach conditions. The temperature dependant bandpass of windows created with present technology, such as single crystal sapphire or aluminum oxynitride (AlON), limits their performance under the necessarily severe operating conditions. The nature of porous optically transparent Type VI gel-silica has previously been reported [3]. It is felt that transpiration of gases through the interconnecting permeable structure of a guidance system window made of Type VI gel-silica should provide a significant cooling effect, thus increasing the working performance of the hypersonic rocket.

Previous work in this area by the authors includes the demonstration of UV transmission at elevated temperatures (>1000°C) [1], evidence of significant transpiration velocities up to 3 cm/sec, and demonstration of a

cooling effect due to the transpiration of He[2]. However, the previous experimental set-up did not permit achieving the conditions necessary to prove that the flows and cooling observed were sufficient for transpiration cooling, as generally defined[4]. Due to the sample testing conditions, the permeabilities of these earlier samples could not be inferred from the measured flow data. It is the intent of this paper to determine the gas permeabilities of several Type VI gel-silica monolithic samples, with an average pore radius of approximately 5 nm, to different gasses. This information will aid in the determination of the flux regime for the windows.

The diffusion or permeation of a fluid, gas or liquid, through a porous solid involves two basic resistances to the net flow velocity of a given species. These are molecule-molecule and molecule-wall interactions. The part each of these interactions play in determining the flux of a species is dependent on parameters of both the fluid and the porous network.

Parameters of the porous network which can play a large part in determining the flux include the effective porosity (interconnected porosity), pore size of the channels, pore size distribution, specific surface area (ratio of the internal surface area to volume), tortuousity of the channels and surface roughness of the channel, to name a few. Important parameters of the fluid include properties such as viscosity, temperature and the molecular weight of the species.

Perhaps the first step in the study of gas flow through a microporous solid starts with a comparison of the mean free paths of the gas (λ) to the average pore size (d) of the media. There is little debate concerning the determination of λ for different gaseous molecules under various flow conditions. The kinetic theory of gases relates λ (of a perfect gas) to the mean speed of a molecule, c, and the collision frequency, z:

2

$$\lambda = c/z = (1/2^{1/2}\sigma)kT/P \qquad\qquad (1)$$

where σ is the collision cross section, k is Boltzman constant, T is the temperature and p is the pressure [5]. It is much more difficult however, to decide upon the appropriate description of the pore size relevant to a specific molecule, flux regime and the correct method of pore size measurement. With the complexity of the interconnected pore space in porous gel-silica monoliths the pore size should be expressed as, at the least, a pore size distribution. Scheidegger points out the difficulty of assigning a value to the pore size because of the random converging and diverging of the normal cross-section of the pores [6]. With this difficulty in mind, it is still desirable to have a measurable parameter which is indicative of the average "size" of the void spaces, i.e., the average pore radius. Perhaps the most common description of the average pore size in a porous media is the hydraulic radius, r_h, defined as twice the pore volume divided by the surface area. Other common methods of determining the pore size are by optical and electron microscopy, mercury injection, and particle rejection methods [7]. The method used herein to obtain the hydraulic radius and pore size distribution is isothermal nitrogen gas adsorption interpreted using the BET (Brunauer, Emmett, and Teller) theory.

The regimes of the various types of gas transport as related to the mean free path (λ) and pore size (d) are found in Table 1 [8].

In the viscous regime of gas flow, resistance to flow is dominated by intermolecular collisions and the velocity profile of the gas flow reaches zero at the wall. One of the fundamental theories applicable to incompressible viscous fluid flow is that of Navier and Stokes [6]. When the velocity of the gas is low throughout the system compared to the speed of sound in the gas, then the flow can be treated as incompressible [9]. We can apply the

Table 1. Regimes of gas flow in microporous structures [8].

Relation	Mechanism	Restriction to Flow
$\lambda \ll d$	Viscous	Molecule-Molecule collisions dominate
$\lambda \simeq d$	Slip	Molecule-Wall-Molecule intermediate
$\lambda \gg d$	Knudsen	Molecule-Wall collisions dominate
$d_m^* \simeq d$	Configurational	

* - molecular diameter

commonly accepted hypothesis known as the Dupuit-Forchheimer assumption to obtain the average velocity of the fluid through the pore space relative to the velocity at the surface:

$$v = q/\varepsilon \qquad (2)$$

where v is the average pore velocity, q is velocity at the surface and ε is the porosity. With the speed of sound in air being approximately 30,000 cm/sec, it is safe to assume that the flow velocities of less than 10 cm/sec can be treated as incompressible even with porosities as low as 10%.

The Navier-Stokes equation has been solved explicitly for straight and circular tubes under the conditions of laminar flow leading to the popular Hagen-Poiseulle equation for viscous flow[6]. Rowell and Bethune give an equation for Poiseuille flow through a porous structure [10]:

$$F_p = \frac{\varepsilon U_o r^2}{8 \eta RTL} \qquad (3)$$

where U_p, r, η, R, T and L are the viscous geometric factor, pore radius, gas viscosity, gas constant, temperature and media thickness respectively. The flow conditions leading to a transition from laminar flow to turbulent flow in

4

dynamically similar systems can sometimes be predicted using the Reynolds number (Re) as defined by:

$$Re = rVP/\eta \qquad (4)$$

where r, V and P are the radius, velocity and pressure respectively. It has been found that for smooth, straight tubes, the critical Re at which the transition can be expected is in the neighborhood of 2200, above which yields turbulent flow [6]. It is important to note that this value changes greatly in the presence of curved tubes. Streeter gives a value of 1 as "a good rule of thumb" for the critical Re of a porous media [11]. With the highly tortuous pore space of a the porous Type VI gel-silica even this value can be much too high, leading to erroneous predictions of laminar flow in this microporous media.

As shown in Table 1, gas flow is considered to be in the Knudsen regime when the mean free path is much greater than the pore size of the porous media. Under this condition resistance to flow is dominated by molecule-wall collisions. It was noted by Knudt and Warburg that this type of molecular flow exhibits a "slip" condition such that the velocity does not equal zero at the wall [6]. It was Knudsen who postulated that the flow rate was a function of not only the pore size and pressure, but also the mean free path of the gas. A corresponding equation for Knudsen gas flow through an isotropic, microporous structure is given by [10]:

$$F_k = \frac{2\varepsilon U_k r_h}{3RTL} \left(\frac{8RT}{\pi m^{1/2}} \right)^{1/2} \qquad (5)$$

where U_k and m are the Knudsen geometric factor and the molecular weight of the gas respectively. The other terms are as defined above.

The slip regime is intermediate to that of viscous and Knudsen. When the mean free path is close to the pore size there are resistive collisions due to both intermolecular collisions and molecule-wall collisions. This results in a velocity at the pore wall intermediate between free slip and zero.

The mean free paths of several gases are presented in Fig. 1. Figure 1 also shows a typical pore size distribution obtained from a porous Type VI gel-silica window with an average pore radius of 5.0 nm. It is apparent that for transpiration of gases at pressures ranging from atmospheric to >500 PSI at least three different gas phase flow mechanisms can possibly account for a portion of the total flux.

Another flow mechanism which can contribute to a substantial increase in flux is surface diffusion, i.e. gases are adsorbed onto the surface of the pore wall and diffuse under a concentration (pressure) gradient. The actual mechanics of surface flow can be very complicated and has been investigated in many papers [12-13]. Due to the limited scope of this paper, only gas phase flows will be considered. The test gases and conditions have been chosen to

Figure 1.   a) Mean free molecular paths verses pressure for several gases
            b) Typical pore size distribution for a sample with a 5.0 nm r_h

promote minimal interaction between the highly polar surfaces of the gel-silica and the gases.

EXPERIMENTAL PROCEDURE

The sol-gel monoliths used in this study were produced using the alkoxide precursor TMOS with an HF catalyst in a procedure described elsewhere[1]. The experimental apparatus to determine the flow rates and permeabilities has also been described elsewhere [2]. A modification to the sample mounting procedure was applied to eliminate the dead volume of the sample, allowing the entire flat surface to be used for flux in and out of the sample. The steady-state pressure drop method was used to determine permeabilities with the low pressure side at atmospheric pressure. Two reasons for using this method include the need to simulate actual use conditions and the longer time necessary to reach an equilibrium steady state flux in the relatively thick (1.4-2.2 mm) samples tested. The volumetric flux was measured using a soap bubble flow meter with graduations of 1, 10 and 100 mls. All permeability measurements were taken at 26°C. Ultra-high purity gases were used where available and research grade otherwise. Pressures were measured with a grade 3-A 4 inch test gauge accurate to $\pm$ 0.25%. The pore morphology, i.e., average pore radius, multipoint BET surface area, and volume fraction porosity were determined using isothermal nitrogen adsorption isotherms obtained on a Quantachrome Autosorb-6.

RESULTS

Permeability measurements of porous gel-silica samples with H_2, He, Ne, N_2, O_2, Ar and Kr as test gases have been performed. Table 2 gives morphological data on the samples tested in this study as well as their permeability (P_{He}) to He. The permeability of sample A has been tested for

7

all the gases listed above. It has a average pore radius of 5.0 nm, porosity
of 67% and a surface area of 367 m^2/g.

Table 2. Properties of Type VI gel-silica monoliths

Sample	Tmax (°C)	A (cm^2)	L (cm)	r_h (nm)	SA (m^2/g)	Vp (cc/g)	ε (%)	P_{He} (X10^4) (cm^3-cm/cm^{2}sec-kPa)
A1	180	1.69	0.20	5.0	367	0.909	66.7	1.15
A2	180	1.67	0.14	5.4	356	0.955	67.8	1.21
A3	180	1.72	0.18	5.3	361	0.965	68.0	1.15
A4	180	1.83	0.22	5.7	358	1.026	69.3	1.34

Figures 2 and 3 show the flow (units r:duced from $cm^3 \cdot cm/cm^2 \cdot sec$
(vol·thick/area·time) to cm^2/sec) of various gases including H_2, He, Neon and
N_2 through sample A1. The linearity of the plots indicate that the flux is
proportional to the pressure as expected for non-turbulent viscous, slip, or
Knudsen flow.

Permeabilities resulting from viscous flow will have a linear pressure

Figure 2.   Pressure dependence of a) H_2 and b) He flow through sample A1.

Figure 3.   Pressure dependence of a) Ne and b) Ar flow through sample A1.

dependency, i.e. permeability increases with mean pressure across the sample,

while permeabilities resulting from Knudsen flow should not be affected by a

change in the mean pressure [6].   Figure 4 shows that for all gases, the

permeabilities through the gel-silica are virtually independent of the mean

pressure, within experimental error. This indicates that Knudsen diffusion is

the dominant mechanism of flow for the combination of samples and conditions

tested here.

Equation 5 shows that for Knudsen diffusion the permeabilities should

vary linearly with the inverse square root of the molecular weight of the gas.

This relationship is due to the dependency of the mean free path upon the

average velocity of the gas molecules. In the case of viscous flow, apparent

from eq. 3, an inverse linear relationship is expected between the

permeability and the gas viscosity. Figure 5 shows the permeabilities of

sample A1 for the various gases plotted against the square root of their

molecular weight. The high correlation observed is also indicative of Knudsen

diffusion being the dominant transport mechanism. Figure 6 shows the lack of

Figure 4.   Dependence of gas permeabilities upon mean pressure.

correlation between the permeabilities and the viscosities of the various gases. The combination of high viscosity, relatively low molecular weight and chemical inertness of neon makes it an ideal gas for comparing Knudsen vs viscous flow.

The data (Figs. 5 and 6) shows that the flow of the various gases through the porous gel-silica samples in this study can be explained by Knudsen diffusion alone. If we assume that eq. 5 is a proper description of Knudsen flow and surface flow is negligible, we still have two terms that are not readily measured or calculated; the average pore radius (for aforementioned reasons) and the sample geometric factor (used interchangeably, and perhaps improperly [6], with 1/tortuousity by many authors).

We can solve equation 5 for all the gases and a given sample to obtain :

$$r_h * U_k = \text{constant} \qquad\qquad (6)$$

Due to the linearity of Fig. 5, this constant should be approximately the same for all gases. For sample A1, this constant has a value of 2.1×10^{-9}m. Using

Figure 5.   Dependence of the permeability on the inverse square root of the
            molecular weight of the gas.

Figure 6. Lack of dependence of permeability upon viscosity.

the BET value of 5.0 nm for the average pore radius a geometric factor of 0.42

is obtained (a tortuousity factor of 2.4 if one wishes to view it as such).

(/

Due to the very tortuous nature of this media and the high degree of surface roughness this factor is quite reasonable.

It is important to note that the permeability values obtained are true permeabilities only if they are independent of the sample thickness. Figure 7 shows the permeation flux (normalized to thickness) of He through four samples with similar pore morphologies but varying thickness, ranging from 1.4 to 2.2 mm thick. The permeabilities, taken from the slopes of these curves are shown to be constant within the experimental error and inherent differences of the samples (Table 2).

Figure 7.   Constant permeability with varying thickness.

CONCLUSION

The purpose of this study was to investigate the gas phase flow through selected samples of Type VI porous gel-silica monoliths. The permeabilities

12

of various gases (H_2, He, Ne, N_2, O_2, Ar, Kr) were measured at room temperature. The permeabilities were found to be independent of the mean pressure and to vary with the inverse square root of the molecular weight of the gas. The flows could be explained by the Knudsen regime alone. Permeability values were found to range from a low of 2.7 x 10^{-5} for Kr to a high of 14.7 x 10^{-5} $cm^3 \cdot cm/cm^2 \cdot sec \cdot kPa$ for H_2.

Future directions should include temperature studies to determine the effect of surface diffusion. In addition, permeabilities through a variety of gel-silica samples with varying pore morphologies may make it possible to determine the proper geometric factor from measurable quantities such as interconnectivity[14], surface area, porosity, pore size, etc.

REFERENCES

1.   L.L. Hench and A.G Fosmoe II, Multifunctional Silica Optics, Mat. Res. Soc. Symp. Proc., Vol. 175, MRS, Pa, 1989.

2.   A.G Fosmoe II and L.L. Hench, Transpiration Cooled Porous Type VI Silica Rocket Windows, Mat. Res. Soc. Symp. Proc., Vol. 180, MRS, Pa, 1990, 843.

3.   L.L. Hench, S.H. Wang and J.L. Nogues, Gel-Silica Optics, in Multifunctional Materials, R.L. Gunshor, Ed., SPIE: Bellingham, Wa, 1988, 878, 76.

4.   U. Kurzweg, private communication.

5. P.W. Atkins, Physical Chemistry, W.H. Freeman and Co., New York, 1986, p. 653.

6. A.E. Scheidegger, The Physics of Flow Through Porous Media, University of Toronto Press, Toronto, 1974.

7. P.C. Carman, Flow of Gases Through Porous Media, Academic Press Inc., London, 1956.

8. R.E. Cunningham and R.J. Williams, Diffusion in Gases and Porous Media, Plenum Press, New York, 1980.

9. D.J. Tritton, Physical Fluid Dynamics, Clarendon Press, 1988.

10. R.L. Rowell, S.A. Carrano, A.J. deBethune and A.P. Malinauskas, Gas and Vapor Permeability, Journal of Colloid and Interface Science, 37, 1971, 242-246.

11. V.L. Streeter, Handbook of Fluid Dynamics, McGraw-Hill, New York, 1961.

12. H. Tamon, S. Kyotani, H. Wada, M. Okazaki and R. Toei, Surface Flow Phenomenon of Adsorbed Gases on Activated Alumina, J. Chem. Eng. Jpn., 14, 1981, 136-141.

13. E.R. Gilliland, R.F. Baddour, G.P.Perkinson and K.J. Sladek, Diffusion on Surfaces. I. Effect of Concentration on the Diffusivity of Physically Adsorbed Gases, Ind. Eng. Chem. Fundam., 13, 1974, 95-99.

14. W. Vasconcelos, Ph.D. dissertation, Univ. of Florida, 1989.

Figure Captions

Figure 1.   a) Mean free molecular paths verses pressure for several gases
             b) Typical pore size distribution for a sample with a 5.0 nm r_h

Figure 2.   Pressure dependence of a) H_2 and b) He flow through sample A1.

Figure 3.   Pressure dependence of a) Ne and b) Ar flow through sample A1.

Figure 4.   Dependence of gas permeabilities upon mean pressure.

Figure 5.   Dependence of the permeability on the inverse square root of the
             molecular weight of the gas.

Figure 6.   Lack of dependence of permeability upon viscosity.
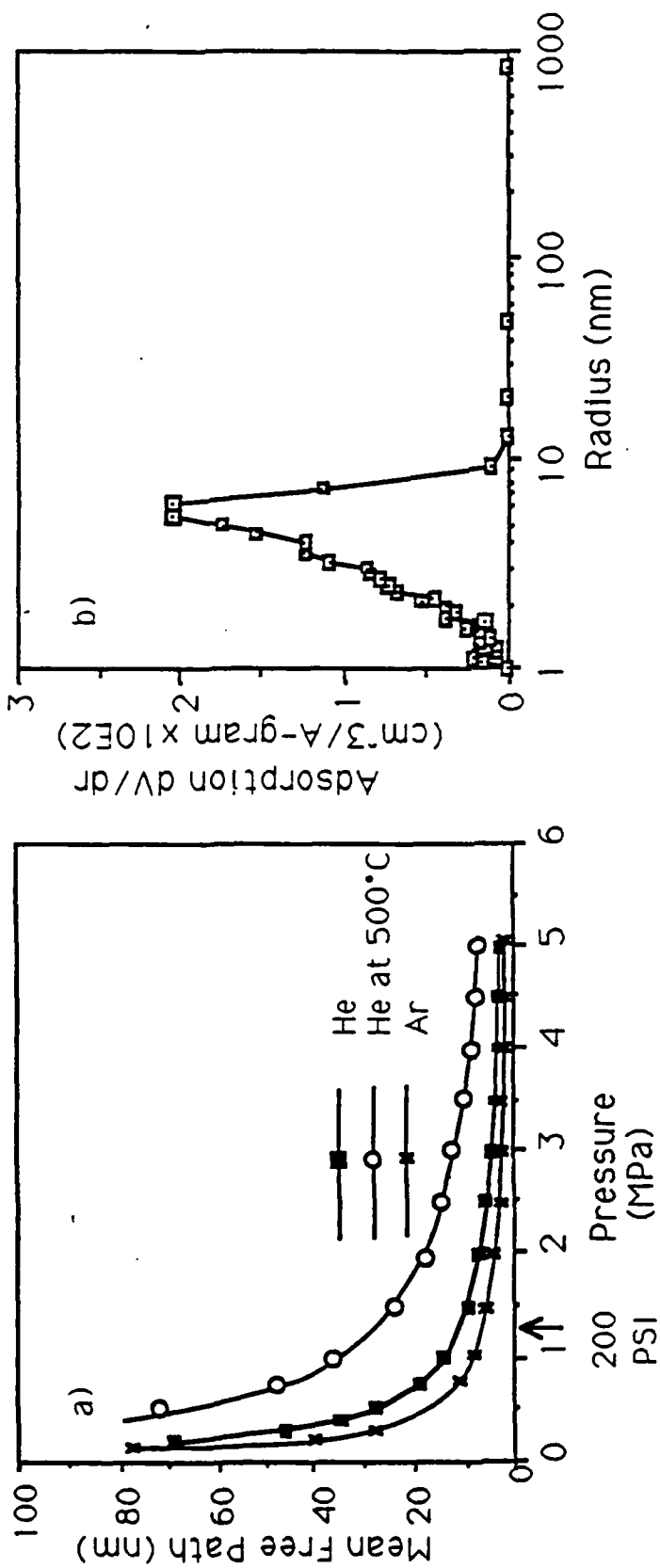
Figure 7.   Constant permeability with varying thickness.

a)
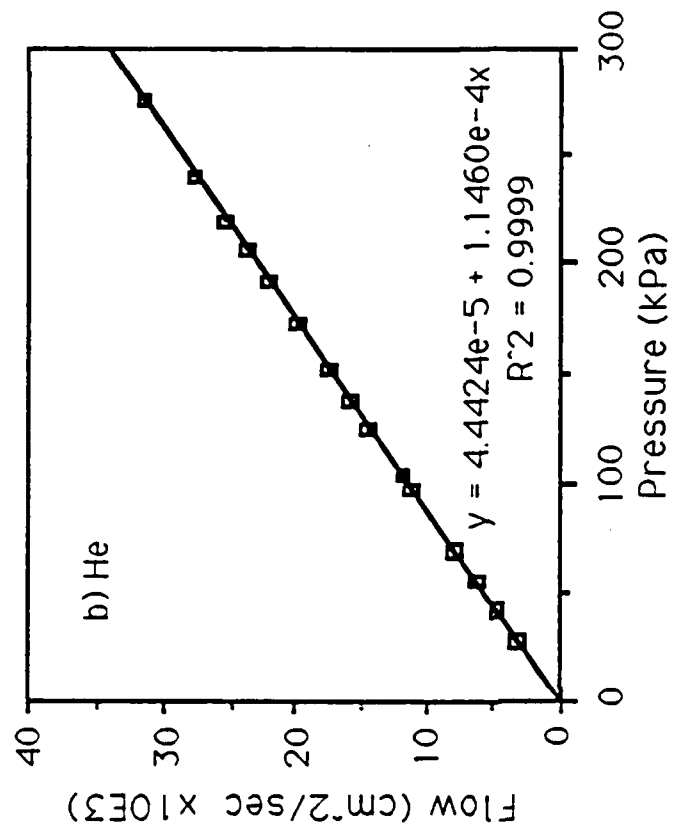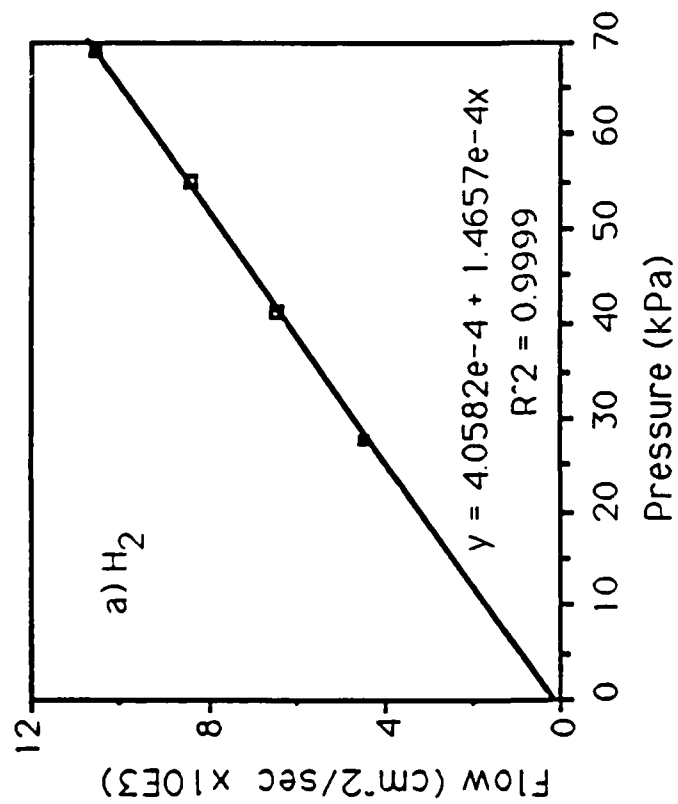
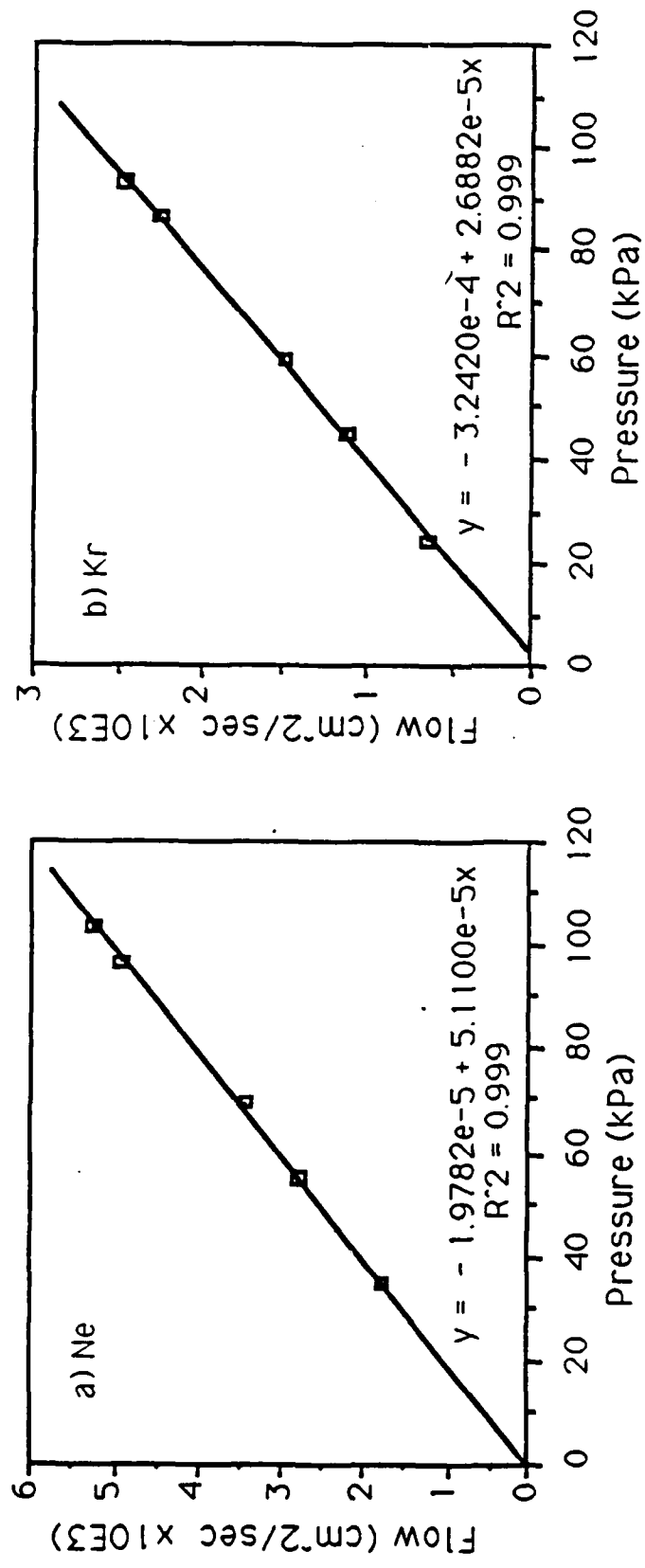Mean Free Path (nm)

Pressure (MPa)

He
He at 500°C
Ar

200 PSI

b)

Adsorption dV/dr (cm³/A-gram ×10E2)

Radius (nm)

Fig. 1

b) He

$y = 4.4424e-5 + 1.1460e-4x$
$R^2 = 0.9999$

Flow (cm²/sec x10E3)

Pressure (kPa)

a) H_2

$y = 4.0582e-4 + 1.4657e-4x$
$R^2 = 0.9999$

Flow (cm²/sec x10E3)

Pressure (kPa)

Fig. 2

a) Ne

$y = -1.9782e{-}5 + 5.1100e{-}5x$
$R^2 = 0.999$

b) Kr

$y = -3.2420e{-}4 + 2.6882e{-}5x$
$R^2 = 0.999$

Fig. 3

Fig. 4

$y = 0.45555 + 20.670x$

$R^2 = 0.995$

Hydrogen

Helium

Neon

Nitrogen

Argon

Oxygen

Krypton

$1/\sqrt{mw}$

Permeability
(cm^2/s-kPa x10E5)

Fig. 5

Fig. 6

Fig. 7

Pressure (kPa)

Flow (cm^2/sec)

A2 (0.14 cm)
A3 (0.18 cm)
A1 (0.20 cm)
A4 (0.22 cm)